universität wien

MASTERARBEIT / MASTER'S THESIS

Titel der Masterarbeit / Title of the Master's Thesis

„Tau Ubiquitination and Condensate Formation with Autophagy Cargo Receptors p62 and NBR1"

verfasst von / submitted by

Yue Qiu, BSc

angestrebter akademischer Grad / in partial fulfilment of the requirements for the degree of

Master of Science (MSc)

Wien, 2021 / Vienna, 2021

Studienkennzahl lt. Studienblatt / degree programme code as it appears on the student record sheet:	UA 066 834
Studienrichtung lt. Studienblatt / degree programme as it appears on the student record sheet:	Masterstudium Molekulare Biologie
Betreut von / Supervisor:	Univ.-Prof. Dipl.-Biol. Dr. Sascha Martens, Privatdoz.

Table of Contents

Abstract

Autophagy is a conserved, lysosome dependent degradation pathway which mediates the removal of unnecessary or dysfunctional components from the cytoplasm. It has become clear that autophagy is also capable of selective degradation of specific proteins and protein aggregates. Tau is a highly regulated axonal cytosolic protein whose pathological accumulation and aggregation can result in neurofibrillary tangle (NFTs) formation. NFTs were shown to colocalize with regions of neurodegeneration in human brain, and therefore interpreted as a hallmark of neurodegenerative Tauopathies including Alzheimer's disease (AD). Degradation of Tau was shown to be greatly reduced by autophagy impairment, suggesting that autophagy may be an effective degradation route for Tau. In this work, I showed that different E2/E3 combinations can attach different patterns of ubiquitin chains on Tau. Ubiquitinated Tau can be specifically recognized by autophagy cargo receptors p62 and NBR1, and the clustering of the three can lead to the formation of condensates. A reproducible procedure was established for the purification of ubiquitinated Tau, and for the microscopic observation and the quantification of condensate formation. Different truncations of p62 and NBR1 were also tested to understand the mechanism behind condensate formation. This work provided the foundation for further research on autophagy degradation of ubiquitinated Tau.

Zusammenfassung

Autophagie ist ein konservierter, lysosomabhängiger Abbauweg, der die Entfernung unnötiger oder dysfunktionaler Komponenten aus dem Zytoplasma vermittelt. Es hat sich herausgestellt, dass die Autophagie auch zum selektiven Abbau bestimmter Proteine und Proteinaggregate befähigt ist. Tau ist ein stark reguliertes axonales zytosolisches Protein, dessen pathologische Akkumulation und Aggregation zur Bildung von neurofibrillären Knäueln (NFTs) führen kann. Es wurde gezeigt, dass NFTs mit Regionen der Neurodegeneration im menschlichen Gehirn kolokalisieren und daher als Kennzeichen neurodegenerativer Tauopathien einschließlich der Alzheimer-Krankheit (AD) interpretiert werden. Es wurde gezeigt, dass der Abbau von Tau durch eine Beeinträchtigung der Autophagie stark reduziert wird, was darauf hindeutet, dass die Autophagie möglicherweise ein effektiver Abbauweg für Tau ist. In dieser Arbeit habe ich gezeigt, dass verschiedene E2/E3-Kombinationen unterschiedliche Muster von Ubiquitinketten an Tau anlagern können. Ubiquitiniertes Tau kann spezifisch von den Autophagie-Cargo-Rezeptoren p62 und NBR1 erkannt werden, und die Anhäufung der drei kann zur Bildung von Kondensaten führen. Zur Reinigung von ubiquitiniertem Tau sowie zur mikroskopischen Beobachtung und Quantifizierung der Kondensatbildung wurde ein reproduzierbares Verfahren etabliert. Verschiedene Verkürzungen von p62 und NBR1 wurden ebenfalls getestet, um den Mechanismus hinter der Kondensatbildung zu verstehen. Diese Arbeit bildete die Grundlage für weitere Forschungen zum Autophagie-Abbau von ubiquitiniertem Tau.

Introduction

Autophagy in general

Autophagy is a conserved, lysosome dependent pathway which enables the routinely removal of unnecessary or dysfunctional components from the cytoplasm. It is essential for maintaining the homeostasis of the cells and has been implicated in various diseases such as cancer and neurodegeneration. Autophagy is a generic term and three types of autophagy have been so far identified: macroautophagy, microautophagy and chaperone-mediated autophagy (CMA)[1,2], among which macroautophagy (hereafter referred to as autophagy) is the most extensively studied pathway.

Autophagy is involved in various biological processes including development, programmed cell death, immune response, and prevention of neurodegeneration[3–5]. Upon induction with starvation and other stresses, crescent-shaped isolation membranes expand to sequester a small portion of the cytoplasm including proteins and organelles[6] (Figure 1). This membrane will keep expanding depending on lipid transfer from endoplasmic reticulum (ER) or other membrane organelles, which after fission leads to the formation of a cargo enclosing double membrane vesicle called autophagosomes[7]. Subsequently, autophagosomes fuse with lysosomes, exposing their inner compartment to lysosomal hydrolases, resulting in the degradation of both the inner membrane of the autophagosome and the enclosed cargo. Through lysosomal membrane permeases, the macromolecules produced by degradation are released into the cytosol and recycled for further use[8].

Autophagy and the ubiquitin-proteasome system (UPS) are the major protein quality control mechanisms that regulate cellular homeostasis in eukaryotes. For many years, the UPS has been considered as the regulator for degradation of specific target proteins, while autophagy was considered responsible for bulk degradation upon induction. However, more evidence has shown that through ubiquitin tags on the cargo, both the UPS and selective autophagy recognize their targets specifically. The UPS mainly eliminates short-lived and soluble misfolded proteins, whereas autophagy mainly degrades long-lived proteins, insoluble protein aggregates but also structures which are not exclusively proteinaceous such as whole organelles (e.g., mitochondria, peroxisomes) and intracellular parasites[9]. The same protein can thus be degraded by the two different systems (e.g., Tau protein), a decision that is likely context-dependent[10]. Furthermore, there also exists crosstalk and reciprocal regulation mechanisms between these two degradation pathways[11].

Cargo Recognition in Selective Autophagy

Besides the non-selective bulk degradation as a response of the cells to nutrient deprivation[12], strong evidence supports that this process may also be highly specific. Indeed, autophagy can also contribute to intracellular homeostasis by selective degradation of specific proteins, protein aggregates, organelles, and pathogens[13]. Neurodegenerative disorders and cancer were linked to autophagy in various studies[14,15], verifying the important role played by selective autophagy in the regulation of cellular homeostasis.

Three basic criteria distinguish selective autophagy from bulk autophagy: the cargo must be specifically recognized, effectively tethered to a nascent autophagosome, and non-cargo material has to be largely excluded from the autophagosome[6]. This selectivity is mediated by autophagy cargo receptors, such as p62, NBR1, or TAX1BP1[16,17]. In mammalian cells, some of these cargo receptor proteins can recognize their specific cargos through post-translational modifications, mainly poly-ubiquitin chains which are attached to the polypeptide

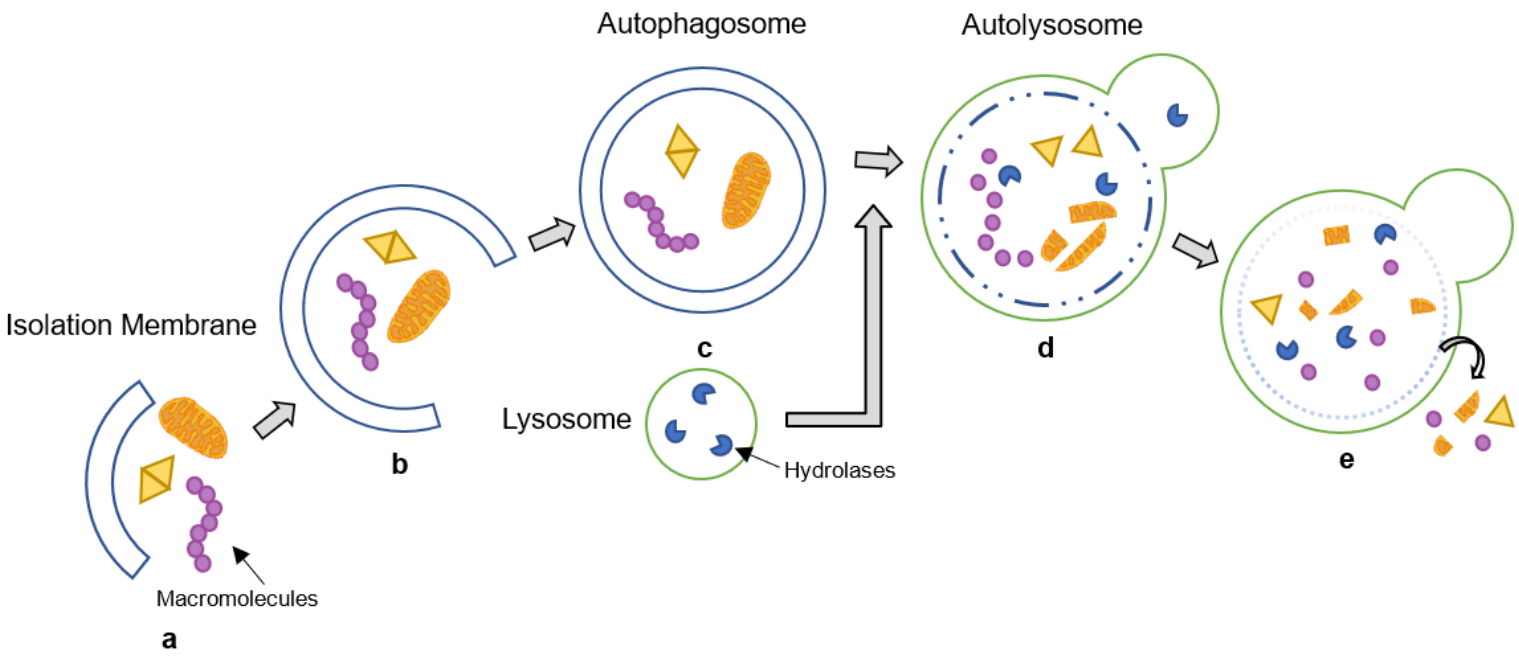

Figure 1: Schematic overview of autophagy.
(a) Initiation of isolation membrane expansion.
(b) Elongating membrane sequesters cytosolic proteins and organelles.
(c, d) Membrane closure leads to formation of a double-membrane autophagosome. The outer membrane fuses with lysosome, exposing the inner membrane and the cargo material to hydrolases.
(e) Degradation of the cargo and recycling of macromolecules.

chains of the cargos[18]. Simultaneously, cargo receptors are capable of binding essential autophagy components such as LC3/GABARAP family proteins (hereafter referred to as LC3) on isolated membranes to tether the cargos to the expanding membrane. Covalent anchoring of LC3 to the membrane is termed as LC3 lipidation, which is associated with phagophore membrane expansion[19].

p62 and NBR1 are mammalian cargo receptors which share a similar domain architecture of an N-terminal PB1 (Phox and Bem1) domain for oligomerization in p62 and protein interaction in NBR1, a LIR (LC3 Interacting Region) motif that interacts with LC3 and a C-terminal UBA (Ubiquitin association) domain that binds ubiquitin[20] (Figure 2). The ubiquitin binding function of the p62 UBA domain is mutually exclusive with its homo-dimerization property, resulting in a relatively low binding affinity with ubiquitinated cargos. In p62, this low affinity can be increased by phosphorylation of serine 403 within the UBA domain, alternatively mimicked by a mutation of serine to glutamate (S403E)[21]. For p62, the dynamic dimerization of UBA domain together with the oligomerization of PB1 might ensure the selectivity for highly ubiquitinated cargos[22,23]. With these properties, p62 can specifically bind to poly-ubiquitinated cargos, and sequentially mediate their clustering into condensates[24,25]. NBR1 acts together with p62 to further promote the formation of ubiquitinated cargo condensates via its PB1 and UBA domains and functions as a crucial regulator[26]. Hence, ubiquitination is a necessary step for the cargo condensation driven by p62 and NBR1.

Furthermore, binding of p62 to certain types of ubiquitin chains attached to the cargo showed a preference that may contribute to the selectivity of autophagy. Multiple ubiquitin can be attached linearly on the methionine at position 1 (M1) or on one of the seven lysine residues (K6, K11, K27, K29, K33, K48, and K63) of a ubiquitin moiety already attached to the target

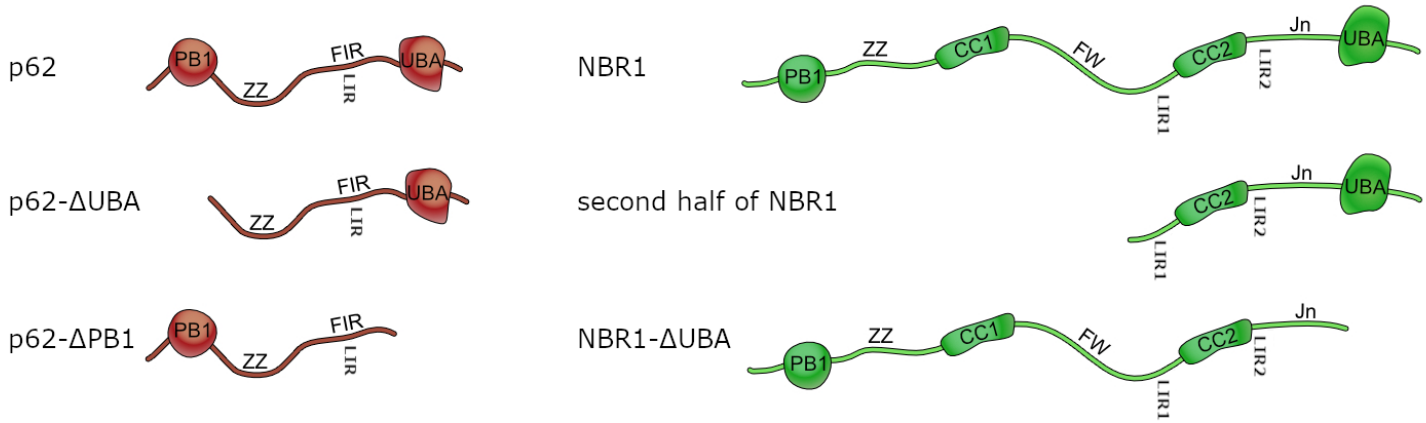

Figure 2: Schematics of the domain organization of the autophagy cargo receptors p62 and NBR1 and the truncations used in this work. ZZ (ZZ-type zinc finger domain), FIR (FIP200-interacting regions), FW (4 tryptophan), cc (coiled coils).

protein, resulting in different chain types[27]. It is known that lysine 48 (K48)-linked chains are often associated with protein UPS degradation, whereas lysine 63 (K63)-linked chains on the cargo tend to target it to autophagy degradation[28,29]. Oligomeric p62 showed preferential binding to linear and K63-linked chains and mono-ubiquitin in comparison to K48-linked chains[23,30]. Similar preference for K63-linked chains has been reported for the UBA domain of NBR1 slightly over K48-linked chains[31]. Moreover, in vitro experiments showed that the binding to unanchored K48-linked free chains disrupts p62 oligomers more prominently than binding to other chain types, which might prevent the degradation of p62 and its cargo through the autophagy pathway[23,32]. However, K48-linked or K63-linked ubiquitin chains used in these in vitro studies were artificial cargos (GFP-ubiquitin, GST-4xUb) that were synthesized in vitro. The effect of ubiquitination on physiological substrates remains largely unknown.

Cargo ubiquitination in selective autophagy

Ubiquitination is an essential signal for the selective degradation of a target protein which is a process accomplished by three enzymes: E1, E2 and E3. RING/U-box E3s catalyzes ubiquitination of the cargo directly from the E2 to the target protein, whereas transfer of ubiquitin by HECT E3s (and RBR ligases) is intermediated by the E2 to an active-site cysteine residue on the HECT E3 ligase before conjugation to the target protein[33]. I focused on the RING/U-box E3s that ubiquitinate target protein in three steps. With each step, one enzyme is involved in catalyzing the translocation of ubiquitin. The first step is the activation of ubiquitin by the enzyme E1 which is an ATP dependent process that links ubiquitin to the E1 via a thioester bond. Secondly, the ubiquitin-conjugating enzyme E2 binds to the complex

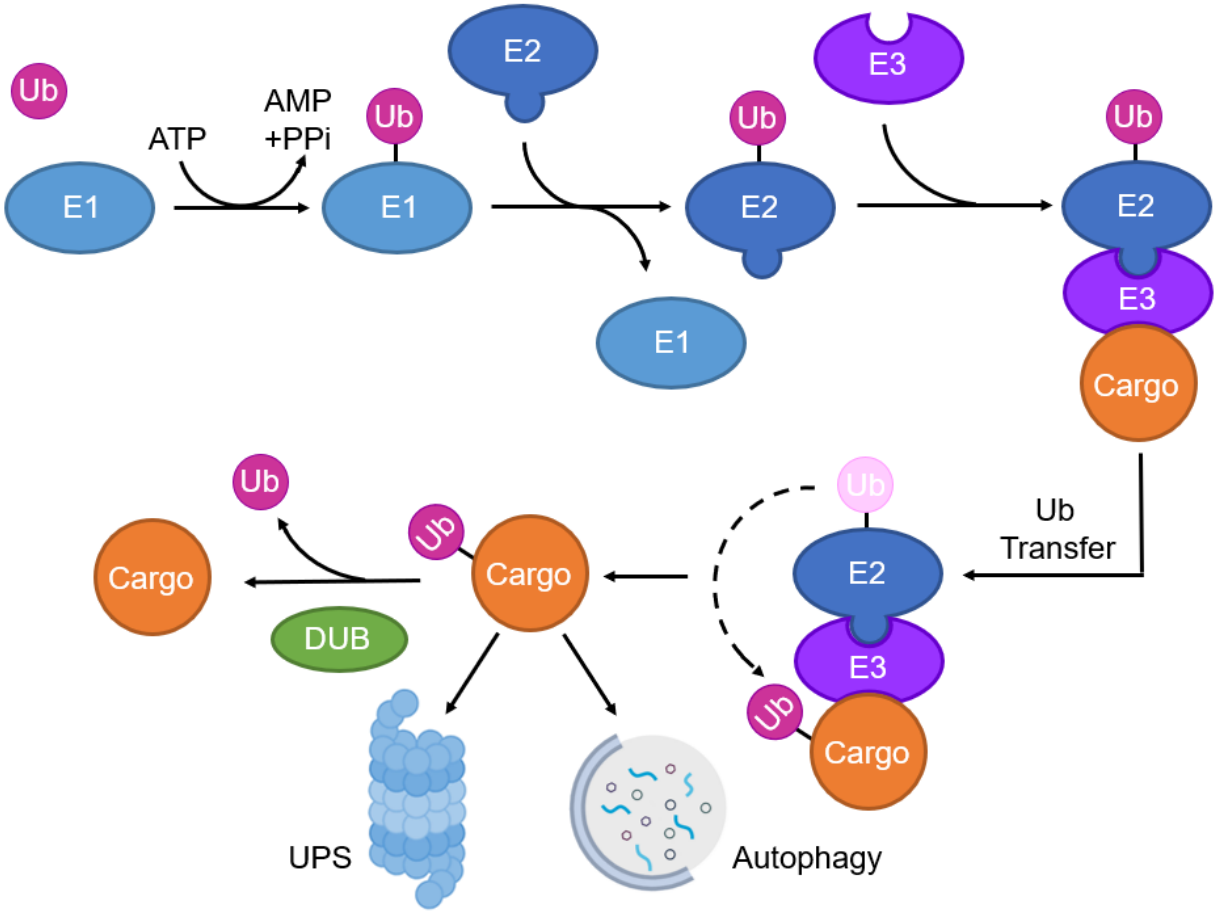

Figure 3: Ubiquitination and de-ubiquitination of autophagy cargos.
Ubiquitin activation by E1 and transferred to E2 subsequently. E3 binds E2-ubiquitin complex and the cargo simultaneously and catalyzes the transfer onto the cargo. Ubiquitinated substrates can also be deubiquitinated with high specificity by DUBs. This reaction is often repeated for the growth of a singly conjugated ubiquitin to the formation of polyubiquitin chains. Adapted from Padraig D'Arcy et al. 2015

formed by activated ubiquitin and E1, and catalyzes the transfer of ubiquitin from E1 to the active site of E2. Finally, the ubiquitination ligase E3 transfer the ubiquitin to lysine residues of substrates or other already attached ubiquitin molecules[34,35]. While E2s determine the specificity for lysine residues, to which ubiquitin will be attached[36,37] the substrate specificity is ensured by E3s that associate with both the substrate and E2-ubiquitin complex[38]. This process is also reversible that a family of enzymes called deubiquitinases (DUBs) can remove ubiquitin from its substrates. DUBs reverse ubiquitin signals by removing ubiquitin from the substrate with equally high specificity as E2 and E3s[39]. (Figure 3)

Tau protein and its degradation through autophagy

Tau is a highly regulated axonal cytosolic protein with major function of binding and stabilizing microtubules in neurons[40]. Tau homeostasis requires a balance of synthesis and degradation, and pathological accumulation and aggregation of Tau can result in neurofibrillary tangles (NFTs) formation. The NTFs ware shown to colocalize with neurodegeneration in human brain and is therefore interpretated as a hallmark of neurodegenerative Tauopathies including the Alzheimer's disease (AD)[41]. Tau tangles were found to correlate with disease progression[42].

Microtubule-associated protein Tau (MAPT) gene coding the Tau protein was found to be expressed in human brain. The protein can be modified by various post translational modifications (PTMs) including phosphorylation, acetylation, glycosylation and oxidation[43]. AD related hyperphosphorylation on serine and threonine residues is mainly clustered in the proline-rich domain (PRD, Figure 4)[44].

It was first generally believed that Tau is degraded by the UPS pathway. However, evidence has shown that UPS might not be the primary pathway for Tau degradation[45,46]. Studies have demonstrated that impairment of autophagy degradation pathway can lead to great reduction of the Tau turnover, thus facilitating the formation of Tau oligomers and insoluble aggregates[47], while autophagy inducers such as rapamycin could reduce this aggregation, alleviate its toxicity and protect against neurodegeneration[48,49]. Different PTM patterns built on Tau could both determine its aggregation propensity and its likelihood to be cleared by autophagy[50].

In AD patients' brain tissues, autophagy cargo receptor p62 was found to colocalize with ubiquitin and aggregate with fibrillary Tau tangles[51,52], which indicates Tau and NFTs are cargos specifically recognized by p62. One study demonstrated that p62 knockout mice acquired age-dependent neuropathy including hyperphosphorylated Tau accumulation and NFT formation, along with cognitive decline[53]. It raised the possibility that the inability of p62 to shuttle polyubiquitinated Tau for degradation to autophagy, or Tau accumulation clustering the p62, resulting in occupation and reduction of accessibility of p62 could be a major causation of disease pathology. As the cargo receptor NBR1 was also found to accumulate in aggregates with p62, ubiquitin, and phosphorylated Tau, it may also play an important role in Tau recognition and degradation[54].

Tau is likely recognized by several E3s, some of them aided by molecular chaperones. Three E3s that specifically recognize and modify Tau have been reported: 1) CHIP (working together with Hsp70 chaperones), driving Tau degradation in cell lines[55,56]. 2) MARCHF7,

found in the NFTs[57] and 3) TRAF6, shown to colocalize in the inclusion bodies isolated from AD patient brain tissue[58]. In combination with different E2s with distinct ubiquitin chain type specificity, a unique pattern of ubiquitin chains can be built on Tau.

In this work, I aim to understand more about the mechanism of Tau recognition and degradation by the autophagy machinery. I characterized the ubiquitination of Tau with CHIP+HSPA1A as E3, in combination with two E2s attaching different ubiquitin chains. I then monitored the clustering of cargo receptors p62 and NBR1 with ubiquitinated Tau through in vitro condensate formation. A reproducible procedure was established for the purification of ubiquitinated Tau, for the microscopic observations of condensates and for their quantification. I demonstrated that the condensate formation of Tau with the autophagy cargo receptor p62 is ubiquitin dependent. The addition of NBR1 significantly facilitated the recognition of Tau and boosted the quantity of condensates, consistent with a former study deploying artificial cargos.[26] The colocalization of all the three components within condensates was shown, and different truncations of p62 and NBR1 were also tested to dissect the contributions of different domains to cargo recognition and clustering.

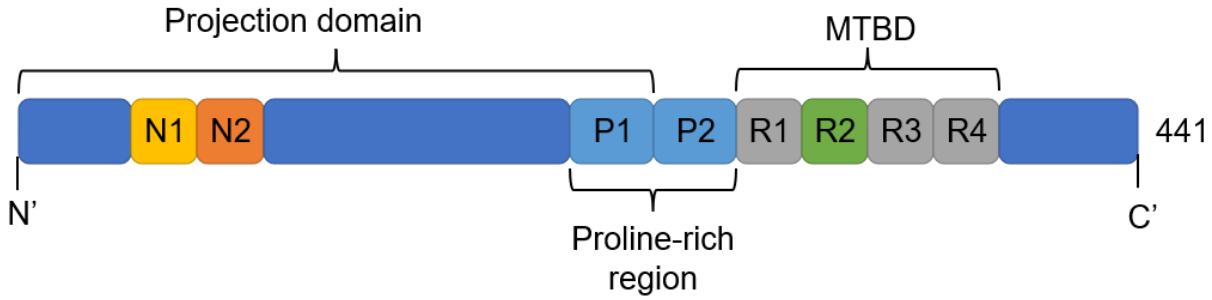

Figure 4: Schematic representation of TAX1BP1 domains
MTBD: Microtubule binding domain

Material and methods

Transformation and cell culture for protein production

EGFP-NBR1 and EGFP NBR1-ΔUBA cloned into FastBac plasmids were already available in the lab and expressed in insect cells. The cloned FastBac plasmid with the gene of interest (GOI) were transformed into electro-competent DH10BacY E. coli (an YFP containing strain) provided by the Thomas Leonard group at the Max Perutz Labs. 1 µL plasmid with a concentration of around 25 ng/µL was electroporated with a Biorad Micropulser with setting for bacteria (two times 5.8 ms at 1.8kV). After recovery at 37°C for 5 hours in Luria broth (LB) medium, cells containing the GOI were plated (blue-white screening on plates with 50 µg/mL Kanamycin, 7 µg/ml Gentamicin, 10 µg/mL Tetracycline, 200 µg/mL X-gal and 165 µM IPTG). White colonies were selected and the recombinants were checked by PCR with insert specific primers M13FW (SMP1770) and M13RV (SMP1771). The verified bacmids were then prepped and used for transfection of the Sf9 insect cells for baculovirus production. The insect cells were cultivated in insect cell culture medium (ESF 921 Expression System LLC) supplemented with Penicillin-Streptomycin at 27°C in humidified 5% CO_2 atmosphere. 800000-1 Million insect cells were plated in one well of a 6-well plate with 2.5 mL of regular media with antibiotics. 2.5 µg of bacmid DNA were transfected with the help of 5 µL FuGENE HD (Promega) and the expression of protein of interest can be directly observed by the expression of YFP. The V0 virus was harvested by collecting the supernatant in the well after 7-8 days and used to transfect a 30 ml insect cell culture. V1 virus was harvested when the viability of cells dropped from almost 100% to 90% and can be stored in 4°C for up to 6 months after filtration. The V1 virus can be used to infect large volumes of cell culture for protein production and the cells were harvested when viability dropped to 90% and pellets can be stored at -80°C.

FLAG-Tau, UBA1, were transformed by heat shock for 45 seconds at 42°C and expressed in E. coli Rosetta cells in 2xTy LB medium containing Ampicillin and Chloramphenicol at 37°C in humidified 5% CO_2 atmosphere. Cells were grown until OD600 reached 0.6–1, induced with 0.15 mM isopropylthiogalactoside (IPTG) and grown at 18°C overnight. Cells were harvested and pellets can be stored at -80°C.

mCherry-p62 S403E, mCherry-p62-ΔPB1, mCherry-p62-ΔUBA, EGFP-C-terminal half of NBR1, UbcH5B, Uev1:Ubc13, MARCHF7 RING domain, CHIP, HspA1A were expressed and purified by colleagues.

Constructs

Protein	Construct code
Flag-Tau	SMC1368
mCherry-p62 S403E	SMC709
mCherry-p62-ΔPB1	SMC544
mCherry-p62-ΔUBA	SMC590
EGFP-NBR1	SMC914
EGFP-C-terminal half of NBR1	SMC1238
EGFP-NBR1-ΔUBA	SMC985
GST-4xUb	SMC538

Table 1: Constructs used for condensation assay

Protein purification

The buffers used in purification of EGFP-NBR1 (SMC914), FL038RR and EGFP-NBR1-ΔUBA are shown in Table 2. Before purification, the pellets were solubilized in 50 mL lysis buffer. The resuspended pellet was driven through a pre-cooled glass Douncer, 10 times with the A pestle and 10 times with the B pestle, and then sonicated (Bandelin Sonoplus) once for 45 seconds with 40% power to lyse the cells. The cell lysate was spun down 40 minutes, 40000 rpm at 4°C. The supernatant was 0.22µM filtered via vacuum pump and loaded on a 5 ml HisTrap column on an ÄKTA FPLC system. The column was pre-equilibrated in buffer A. The imidazole elution of the HisTrap purification consisted of 6 buffer steps with 50mM, 75mM, 100mM, 150mM, 200mM and 300mM of imidazole, 5 column volume each. The peak fractions were checked on SDS-PAGE and collected protein-containing peak fractions were pooled and cleaved with one 25 µL aliquot of His-TEV protease without glycerol overnight rolling at 4°C. The gel filtration column S6 10-300 (not increase) was pre-equilibrated with SEC buffer. The cut product was concentrated to 0.5-1 ml with 100k Amicon Ultra 15 mL centrifugal filter units (Merck) and loaded on size exclusion chromatography (SEC) with 1 mL loop and further separated by size through isocratic elution. The purified protein was concentrated with 100k Amicon Ultra 4 mL centrifugal filter units. Final concentration was determined by Nanodrop A280 and the protein was aliquoted, frozen with liquid nitrogen and stored at -80°C.

Lysis buffer

Reagent (stock)	Volume for 50 mL	Final conc.
HEPES (1 M)	2.5 mL	50 mM
NaCl (5 M)	1.5 mL	150 mM
$MgCl_2$ (1 M)	100 µL	2 mM
CHAPS	125 mg	0.25 %
Protease inhibitor cocktail tablets (Roche, EDTA free)	1 tablet	-
PefaBlock (100 mM)	500 µL	1 mM
Benzonase (Millipore SIGMA)	1 µL	-
DNAse (SIGMA)	a tip	-
RNAse	20 µL	-
Protease inhibitor protease (SIGMA)	150 µL	-
Imidazole (3 M)	166 µL	10 mM
β-Mercaptoethanol (14.3 M SIGMA)	7 µL	2 mM
H_20	to 50 mL	-

HisTrap, Buffer A

Reagent (stock)	Volume for 250 mL	Final conc.
HEPES (1 M)	12.5 mL	50 mM
NaCl (5 M)	7.5 mL	150 mM
Imidazole (3 M)	0.85 mL	10 mM
CHAPS	0.625 g	0.25 %
β-Mercaptoethanol (14.3 M)	35 µL	2 mM
H_20	to 250 mL	-

HisTrap, Buffer B

Reagent (stock)	Volume for 150 mL	Final conc.
HEPES (1 M)	7.5 mL	50 mM
NaCl (5 M)	4.5 mL	150 mM
Imidazole (3 M)	15 mL	300 mM
CHAPS	375 mg	0.25 %
β-Mercaptoethanol (14.3 M)	21 µL	2mM
H_20	to 150 mL	-

SEC buffer

Reagent (stock)	Volume for 500 mL	Final conc.
HEPES (1 M)	12.5 mL	25 mM
NaCl (5 M)	15 mL	150 mM
DTT (1 M)	0.5 mL	1 mM
H_20	to 500 mL	-

Table 2: Purification buffers for EGFP-NBR1 and EGFP-NBR1-ΔUBA. β-Mercaptoethanol and DTT were added immediately before use.

Purification of UBA1 and FLAG-Tau followed similar procedures. Lysis buffer used for UBA1 was shown in Table 3. The cell lysate of UBA1 production was lysed by 3 x 30 seconds sonication with each time of 70% power and 5 cycles, no douncing was needed. The concentration of the purified protein was conducted using a 30k Amicon Ultra centrifugal filtration unit.

Lysis buffer

Reagent (stock)	Volume to 50 mL	Final conc.
HEPES (1 M)	1.25 mL	25 mM
NaCl (5 M)	1.5 mL	150 mM
Imidazole (3 M)	416 µL	25 mM
β-Mercaptoethanol (14.3 M)	7 µL	2 mM
Protease inhibitor	1 tablet	
H_2O	to 50 µL	

Table 3: Lysis buffer for UBA1

For FLAG-Tau, the lysis of cells was the same as UBA1. For its purification, an extra step of cation exchange chromatography was added between the HisTrap and the SEC runs. Buffers of which are shown in Table 4. Fractions collected from HisTrap were concentrated down to 1 ml with 3K Amicon concentrator (pre-equilibrated with SP XL, Buffer A) and diluted with 50 ml of ice-cold buffer of 12.5 mM HEPES + 1 mM DTT, in order to lower the salt and imidazole content. The protein was loaded onto a SP XL 1ml column and the purification fractions containing the Tau protein were collected and cleaved with TEV protease to be loaded on SEC afterwards.

SPXL, Buffer A

Reagent (stock)	Volume to 250 mL	Final conc.
HEPES (1 M)	6.25 mL	25 mM
NaCl (5 M)	2.25 mL	45 mM
DTT (1 M)	250 µL	1 mM
H_20	to 250 mL	-

SPXL, Buffer B

Reagent (stock)	Volume to 100 mL	Final conc.
HEPES (1 M)	2.5 mL	25 mM
NaCl (5 M)	10 mL	500 mM
DTT (1 M)	150 µL	1 mM
H_20	to 100 mL	-

Table 4: Cation exchange chromatography buffer for FLAG-Tau

SDS-PAGE and Coomassie staining

For SDS PAGE analysis, 6x protein loading dye was added to the samples and boiled at 98°C for 5-10 minutes. Purification samples were loaded on polyacrylamide gels (10%-12%). For better separation of ubiquitin chains, commercial gradient gels (Invitrogen Bolt 4-12% Bis-Tris Plus 1.0mm x 15 wells pre-cast gel) were used for samples from ubiquitination assay and FLAG-Tau purification by M2 beads. SDS running buffer diluted from 10x stock was used for normal gels, while MES buffer diluted from 20x stock was used for pre-cast gels. The gels were run at a voltage of 200 – 300 V for 20 – 60 minutes. For molecular weight determination of the proteins, Page Ruler Prestained Protein Ladder (-Plus) (Thermo Scientific) was used as marker. Gels were then stained 5 minutes with Coomassie brilliant blue and destained with 10% acetic acid two time for 10 minutes each. Some gels were used for western blot by skipping the Coomassie staining step.

6x protein loading dye

Reagent (stock)	Volume to 10 mL	Final conc.
Tris-Cl (3 M pH 6.8)	1.25 mL	375 mM
Glycerol 100%	6 g	60%
SDS (Powder)	1.2 g	12%
Bromphenol-Blue sod salt	60 mg	0.6%
H_20	to 8.7 mL	-

Add fresh before aliquoting		
β-Mercaptoethanol (14 M)	1.3 mL	1.8 M

SDS running buffer

Reagent (stock)	Volume to 1 L	Final conc.
Tris (MW=121)	30.25 g	250 mM
Glycine (MW=75)	144 g	1.9 M
SDS (Powder)	10 g	1%
H_20	to 1 L	-

20x MES-SDS running buffer

Reagent (stock)	Volume to 500 mL	Final conc.
MES	97.6 g	1 M
Tris (MW=121)	60.6 g	1 M
EDTA (MW=372 for dihydrate)	3 g	16 mM
SDS (Powder)	10 g	2%
H_20	to 500 mL	-

Table 5: SDS-PAGE and Coomassie staining buffers.

Western Blot

Instead of Coomassie staining, particular proteins (e.g., FLAG-Tau) can be identified by western blot with specific antibodies after SDS-PAGE separation. In order to make the proteins accessible to antibody detection, the protein was transferred from acrylamide gel onto a membrane. The gel was placed in a blotting sandwich with the order of negative pole, foam pad, two layers of filter paper, gel, PVDF 0.2 µm transfer membrane (Thermo Fisher), two layers of filter paper, foam pad, positive pole. The transfer membrane was already activated with methanol for 1-5 minutes before assembling the blotting sandwich. The blotting sandwich was then put in the Bio-Rad chamber and transferred for 90 minutes at 120V in ice box or overnight at 30V 4°C.

The membrane was taken out after the transfer and it was kept in buffer at 4°C if necessary. To continue with antibody detection of the target protein, the membrane was blocked by TBS-3% milk incubation for 60 minutes at room temperature, to prevent the non-specific interactions between the membrane and the antibody.

Primary antibody anti-FLAG (mouse, 6B2 from Ogris Lab) was diluted 1:200 in TBST-3% milk (0.1% tween®20, SIGMA). The membrane was incubated with the primary antibody solution

at 4°C overnight or 1 hour at room temperature. The membrane was then washed three times with TBST, 10 minutes each wash. Secondary antibody goat anti-mouse IgG HRP (Dianova) was diluted 1:10000 in TBST-3% milk and used to incubate the membrane for 45 minutes at room temperature, followed by 2 TBST washes of 10 minutes each. The membrane was developed with 2 ml substrate (1:1 mixture of Clarity Western ECL substrate, Bio-Rad) for 1-5 minutes and imaged directly after.

Band intensity quantification

For the band intensity quantification on SDS-PAGE gel or western blot, an ImageJ plugin was used: _BandPeakQuantification.ijm (https://www.protocols.io/view/quantification-of-gel-bands-by-an-image-j-macro-ba-7vghn3w?step=8)
The gel to be quantified was opened on ImageJ. The color was inverted by choosing “Invert the image” in the “Edit” tab. The regions to be quantified were chosen using “Rectangle selection” and added to the ROI (region of interest) by pressing Ctrl+T. After all the regions were added in to the ROI, the program was started with setting of background width = 3, estimate background from: all, and background estimation by: median. The final result is the “Signal” given by the program which is the band intensity adjusted with the background.

Ubiquitination assay

For the ubiquitination of FLAG-Tau, a total reaction volume of 600 µL was used. The 10x ubiquitination buffer consisted of 250 mM Tris-HCl (pH 7.5), 1200 mM NaCl and 10 mM MgCl2, DTT was added freshly on the day, 0.3 µL of 1 M DTT was added to 100 µL of stock 10x buffer, for a working concentration of 3 mM DTT. The proteins were thawed on hand, spun down 10 minutes at 4°C max speed (14500 g bench centrifuge). This buffer was used for reaction mix. UBA1 was diluted from 40.7 µM to 4.07 µM by adding 2 µL of protein (from supernatant) to 18 µL of SEC buffer. The reaction mix was prepared on ice following Table 6 except for ATP. The reaction was started by adding ATP and tubes were mixed by gently flicking., A sample for SDS-PAGE was taken for the time point 0' and then the reaction mix was put at 30 °C and incubated overnight. In the morning, samples were moved on ice and another sample for SDS-PAGE was taken.

Reagent	Final conc.	Volume (µL)
Water	to 600 µL	319.5
Ubiquitination Buffer 10x	25 mM	60
E1 UBA1 (4.07 µM)	50 nM	7.37
Ubiquitin (822 µM)	100 µM	73
E2 Uev1:Ubc13 (350 µM)	5 µM	8.57
E3 CHIP (µM)	2.5 µM	9.38
HSPA1A (132 µM)	1 µM	4.55
FLAG-Tau (68.5 µM)	10 µM	87.6
ATP pH6 100mM	5 mM	30

Table 6: Ubiquitination reaction mix components.

M2 anti-FLAG bead purification of FLAG-Tau (ubiquitinated and monomeric)

The Anti-FLAG M2 affinity Gel A2220 (Thermo Fisher) can recognize FLAG tag with high specificity. Based on the amount of Tau used, the amount of beads slur necessary to bind Tau was calculated according to the manufacturer's information, and then doubled experimentally to ensure that all FLAG-Tau was collected to minimize protein loss. 0.2 µm filtered SEC buffer (1 M HEPES pH 7.5 375 µL, 5 M NaCl 450 µL, H_2O 14.2 mL) was prepared and 15 µL 1 M DTT to a final concentration of 1 mM DTT was added on the day of the experiment. The ubiquitination reaction (see above) was spun down 10 minutes at 4°C 14500 g. In the meanwhile, the beads were cleaned 4 times with 0.8 mL of SEC buffer, vortexed for 5 seconds, spun down at 7000 g for 60 seconds each time. Supernatant was carefully removed. The Tau ubiquitination reaction (see above) was added to the equilibrated beads, incubated for 60 minutes on roller in the cold room (in 50 mL tube with some paper). Subsequently, the mix was spun down for 60 seconds at 7000 g and the supernatant was removed. The beads were washed three times with 1 mL of SEC buffer, and each time vortexed for 5 seconds, spun down for 60 seconds at 7000 g, and the supernatant was carefully removed.

For Tau elution with a FLAG-peptide (F3290, Thermo Fisher), double molar of FLAG-peptide to Tau was added. The mix was then centrifuged for 30 seconds–1 minute at 5000-8200 g. The supernatant was carefully transferred to a 3.5 kD dialysis membrane (Spectra standard RC tubing) without beads and dialyzed overnight at 4°C. The dialyzed protein was transferred

to a 3kDa cutoff concentrator pre-equilibrated with water and SEC buffer and centrifuged until the remaining volume was around 100 µL. A sample for SDS-PAGE was taken for the final product and the purified protein was aliquoted and frozen in liquid nitrogen.

Microscopy of condensate formation

Proteins were thawn from -80°C and spun down for 10 minutes at 4°C of 16000 rpm. Proteins were diluted to the desired concentrations in the reaction mix (p62: 2 µM, NBR1: 1 µM) and the salt concentration was adjusted with SEC buffer to 160 mM, as p62 was in 500 mM NaCl buffer while the other proteins were in standard 150 mM NaCl buffer. Buffers and diluted proteins were pipetted and mixed directly in a 384 wells plate, making sure that the liquid was distributed homogenously at the bottom of the well.
The reaction was observed and recorded with a Visitron spinning disk microscopy after incubation for the intended length of the experiment (usually 4 hours, or directly after pipetting for kinetics). If kinetics were being measured, the position of the stages was set by first adding double amount of buffer and cargo receptors to have enough amount of liquid covering the bottom of the wells. After setting up the stages to the correct z-level, half of the volume was taken out, substrate was added and the plate was quickly sealed with parafilm, imaging was started immediately after. The camera used was EM-CCD with 20x objective, laser intensity was set to 35% for mCherry and 50% for GFP, exposure 100 ms for mCherry and 150 ms for GFP, and gain 100-150. The stages were chosen in the middle of the wells and stacks of range of 50 µm from the center were taken, ensuring that the images obtained were still in within the suspension. When measuring kinetics, autofocus was selected for time-lapse recording and interval was chosen from 2-5 minutes for the first 1-2 hours and 10 minutes afterwards.

Quantification of condensates

ImageJ plugin “Particle Analyzer v5.ijm” written by Thomas Peterbauer was used for quantification of condensates throughout this work. Images to be quantified were opened in ImageJ and the program was run using the following settings:
var channel=1; //'1' or '2' (more channels are not supported)

var zSlice=1-5; //z slice to process (enter '0' for a maximum intensity projection
var limit=1; //size exclusion limit for particle analyzer (pixel units)
var detailed=false; //optional: detailed results ('true' or 'false')
var skipFirstImages=0; //number of first images to skip ('0' for none)
var filter=true; //applies median filtering with radius 2
var rollingBall=5; //rolling ball radios for background correction
var threshold=190; //set to '0' for autothreshold
var autoThresholdSlice=10; //slice to get the autothreshold
var keepROIs=true; //keeps ROIs of particles in the ROI manager
The settings were constant except that the threshold was changed (normally 180-300). Based on visual comparison of the binarized figures of how many particles were being counted with the original figures, the threshold can be adjusted.

Immunofluorescence staining of condensates

The condensate formation reaction mix was prepared as described in “Microscopy of condensate formation”. The reaction was incubated for 4 hours for maximal condensates to be formed. Primary antibody Mouse anti-Flag (6B2 from Ogris group, Max Perutzt Labs) was added in dilution series of 1:500, 1:2000, 1:20000, 1:200000 (1:200 was used normally in western blot). 10x dilution of primary antibody of 1:50, 1:200, 1:2000, 1:20000 was made and 1 µL of each dilution was added to a 10 µL reaction mix and incubated overnight at 4°C. Secondary antibody goat anti mouse IgG H&L Alexa Fluor 405 was used at a concentration of 1:500 (concentration of 1:250 is recommended for Immunofluorescence). Dilution of 1:50 made and 1 µL was added to a 10µL reaction mix and incubated for another hour. The colocalization of the three fluorophores (mCherry of p62, EGFP of NBR1 and Alexa 405 of Tau) was observed on bottom of the wells and recorded by ZEISS LSM 700 Confocal Laser Scanning Microscope.

Results

Different combinations of E2s and E3s ubiquitinate Tau with distinct chain type patterns and kinetics

In order to test how the autophagy cargo receptors p62 and NBR interact with a physiological, ubiquitinated substrate, and whether Tau can be recognized as autophagy cargo in vitro, I first attempted to produce ubiquitinated Tau. I showed that the ubiquitination of Tau is ATP dependent, and each component in the ubiquitination machinery is indispensable (Figure 5a). To this end, UBA1 was used as E1 throughout this work. Here I used UbcH5B as E2 working together with the MARCHF7 (also known as Axotrophin) RING domain as E3[57], and FLAG tagged Tau as substrate. After 15 minutes, reactions were blocked by addition of protein loading dye and analyzed by western blot using an anti-FLAG antibody. FLAG-Tau with a predicted molecular weight of 46kDa ran at an apparent mass of about 70kDa with degradation bands, as previously reported[59]. Ubiquitin chains were assembled on Tau only when E1, E2, E3, ubiquitin and ATP were all present. Long polyubiquitin chains were assembled in 15 minutes, which indicates that the chain attachment was very efficient. The mass of the individual bands of the ladder increased with discrete steps, roughly corresponding to the molecular weight of one ubiquitin.

I tested another E3, CHIP. This is a E3 with U-box domain[60] that works together with HSPA1A, a major member of the Hsp70 chaperone family. CHIP was identified as a E3 that specifically recognize Tau as substrate[55], while the HSP70 chaperone level was found to inversely correlate with Tau aggregation[61]. It was proposed that these two components work together to control Tau degradation. Through the mass spectrometry analysis (Figure 5b, unpublished data by Luca Ferrari), the specificity of ubiquitin chain types attached to FLAG-Tau by different E2/E3 combinations can be distinguished. Among the combination tested, heterodimeric Uev1:Ubc13 as E2 together with CHIP and HSPA1A as E3 assembled mostly K63-linked chains on Tau, whereas using UbcH5B as E2 with CHIP and HSPA1A as E3 assembled mix chain types including not only K48- and K63-linked chains, but also K-27-linked chains.

I further highlighted the kinetics differences in chain assembly when using HSPA1A and CHIP in the presence of either UbcH5B or Uev1:Ubc13 (Figure 5c, d). While poly- ubiquitination was readily detectable after only 15 minutes for UbcH5B, ubiquitin chains attached to Tau by Uev1:Ubc13 were only observed at the 4 hours' time point. Meanwhile, there was also a great

difference in the amount of ubiquitin attached to single monomeric Tau (Figure 5c). Ubch5B has showed a preference of attaching monoubiquitin over polyubiquitin chains. In contrary, mono- ubiquitination by Uev1: Ubc13 was not detectable on the western blot and three or more ubiquitin attachment were more abundant, possibly highlighting faster kinetics for mono- and di- ubiquitination reactions over polyubiquitination. The overall ubiquitinated portion of monomeric Tau did not increase further after reaching a certain plateau, and the amount of ubiquitinated Tau seemed to be less for Uev1:Ubc13 as estimated from the band intensity.

As K63-linked chains attached to the cargo were shown to associate the cargo with autophagy degradation[29], the combination of Uev1:Ubc13 and CHIP with HSPA1A was considered to be more relevant for our research direction and was used throughout the majority of our following experiments.

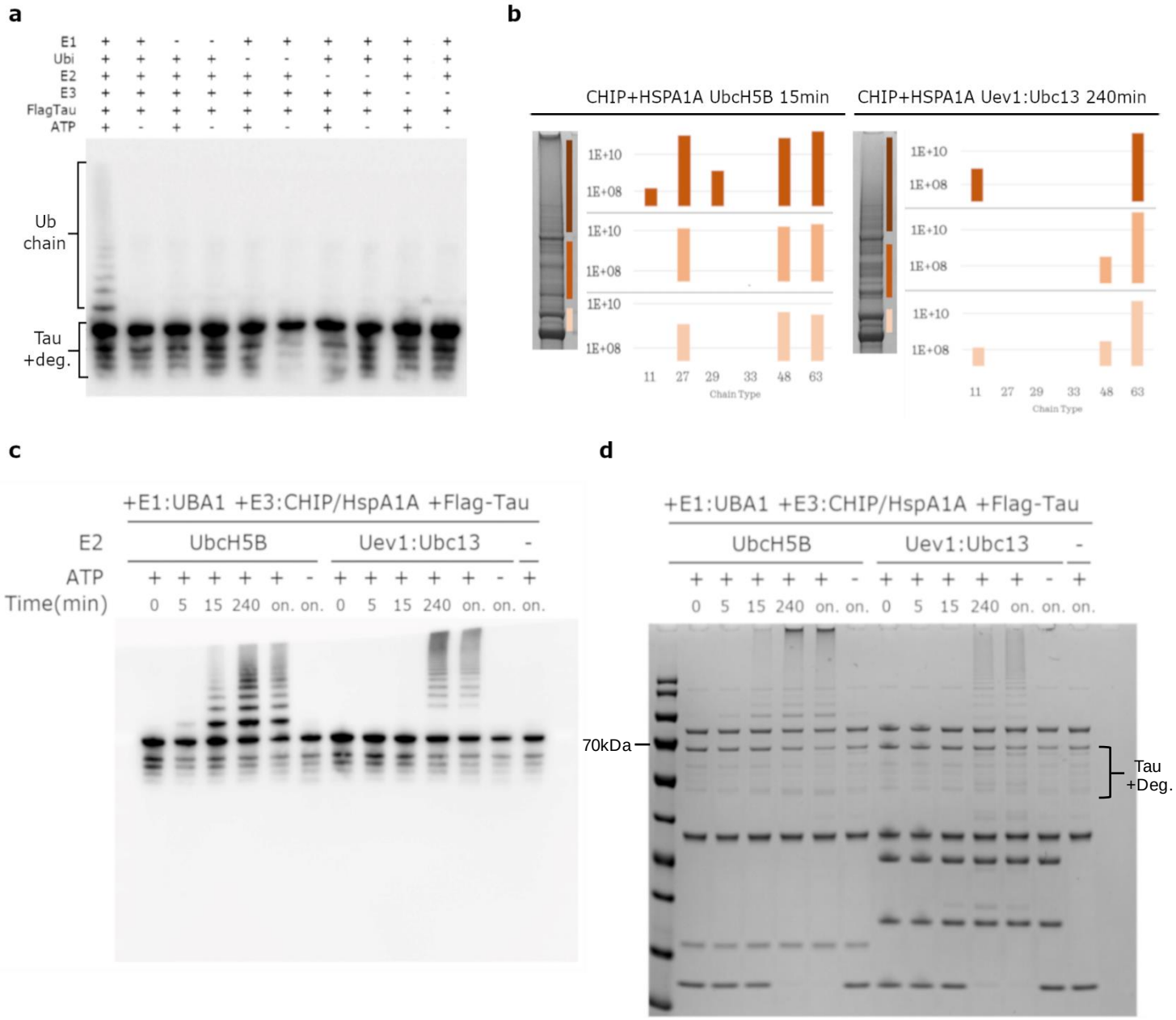

Figure 5: Different E2s determine the ubiquitin chain type assembled on Tau.

(a) Anti-FLAG Western blot following Tau ubiquitination by UbcH5B as E2 and CHIP with HSPA1A as E3. Reactions were performed for 15 minutes.

(b) Mass spectrometry analysis showing which ubiquitin chain types are assembled on Tau by UbcH5B or Uev1:Ubc13.

(c) Anti-FLAG Western blot of Tau ubiquitination by UbcH5B or Uev1:Ubc13 as E2s and CHIP/HSPA1A as E3 over time. Negative control without ATP or E2 are shown.

(d) SDS PAGE of a time course of Tau ubiquitination by UbcH5B or Uev1:Ubc13 as E2s and CHIP/HSPA1A as E3. Negative control without ATP or E2 are shown.

Conditions for all reaction mixes: UBA1 (E1) 50 nM, UbcH5B (E2) 0.5 µM or Uev1:Ubc13 (E2) 5 µM, MARCHF7 RING domain (E3) 2.5 µM or CHIP (E3) 2.5 µM + HSPA1A 1 µM, ubiquitin: 100 µM, ATP:5 mM, FLAG-Tau: 10 µM; salt concentration: 150 mM; all reactions were performed at 30°C.

Establishing a method for the purification of ubiquitinated Tau from the ubiquitination machinery

After verifying the ubiquitination of Tau protein by western blot, I then looked for methods that could efficiently purify Tau from the ubiquitination machinery, as the latter could potentially interact with autophagy cargo receptors, thus making our observations more difficult to interpret (e.g., E2 or E3 conjugated with ubiquitin as well as free ubiquitin chains could also be recognized by p62 and NBR1). Since the Tau protein used in this study is FLAG-tagged, a reproducible purification assay was established and optimized by using anti-FLAG M2 affinity gel beads. (Figure 6)

I first performed the ubiquitination reaction of Tau with Uev1:Ubc13 as the E2 and CHIP/HSPA1A as the E3. Anti-FLAG M2 beads were added to the ubiquitination reaction mix, to ensure full binding of Tau. After incubation, Tau proteins were separated from the rest of the components by centrifugation and washing steps. To elute Tau from the M2 anti-FLAG beads, double amount of FLAG-peptide to Tau protein was added to the solution and incubated at room temperature. The eluted Tau was in mixture with excessive FLAG-peptide and therefore further purified through dialysis and concentrated afterwards.

I noticed that the final purified product still showed a faint band on SDS-PAGE gel corresponding to HSPA1A (which runs at identical position as monoubiquitinated Tau and could not be detected by western blot), indicating co-purification with Tau. HSPA1A binding to its substrate is less efficient when the chaperone is in its ATP-bound state, I thus added an extra step of ATP wash for 30 minutes at room temperature, to release Tau from the HSPA1A chaperone. The ATP wash significantly reduced the amount of HSPA1A in the final product (Figure 6c). The protein was thus pure for further investigation.

The anti-FLAG (Tau) western blot and SDS-PAGE gel of the purification outcome indicates that this procedure achieved the efficient removal of the other components in the ubiquitination reaction mix and is able to increase the total and relative concentrations of monomeric and ubiquitinated Tau (Figure 6b). I estimated Tau concentration by band intensity quantification via ImageJ (Table 7). The “signal” column denotes the background-corrected integrated intensity which eliminates the accidental deviation between images, while the “total” column is the integrated intensity within the ROI selected manually without background correction. The concentration of the purified ubiquitinated Tau is thus calculated based on Coomassie gel bands, comparing the signal of the purified Tau with the input Tau of known concentration. This allowed us to estimate the concentration of purified

ubiquitinated Tau and determine the volume of which to be added in the downstream condensate formation experiments.

Sample	Signal	Total	Concentration
Input	52014	106339	10 µM
Final product	80879	217771	15.5 µM

Table 7: Band intensity quantification for Tau concentration determination in M2 beads purification.

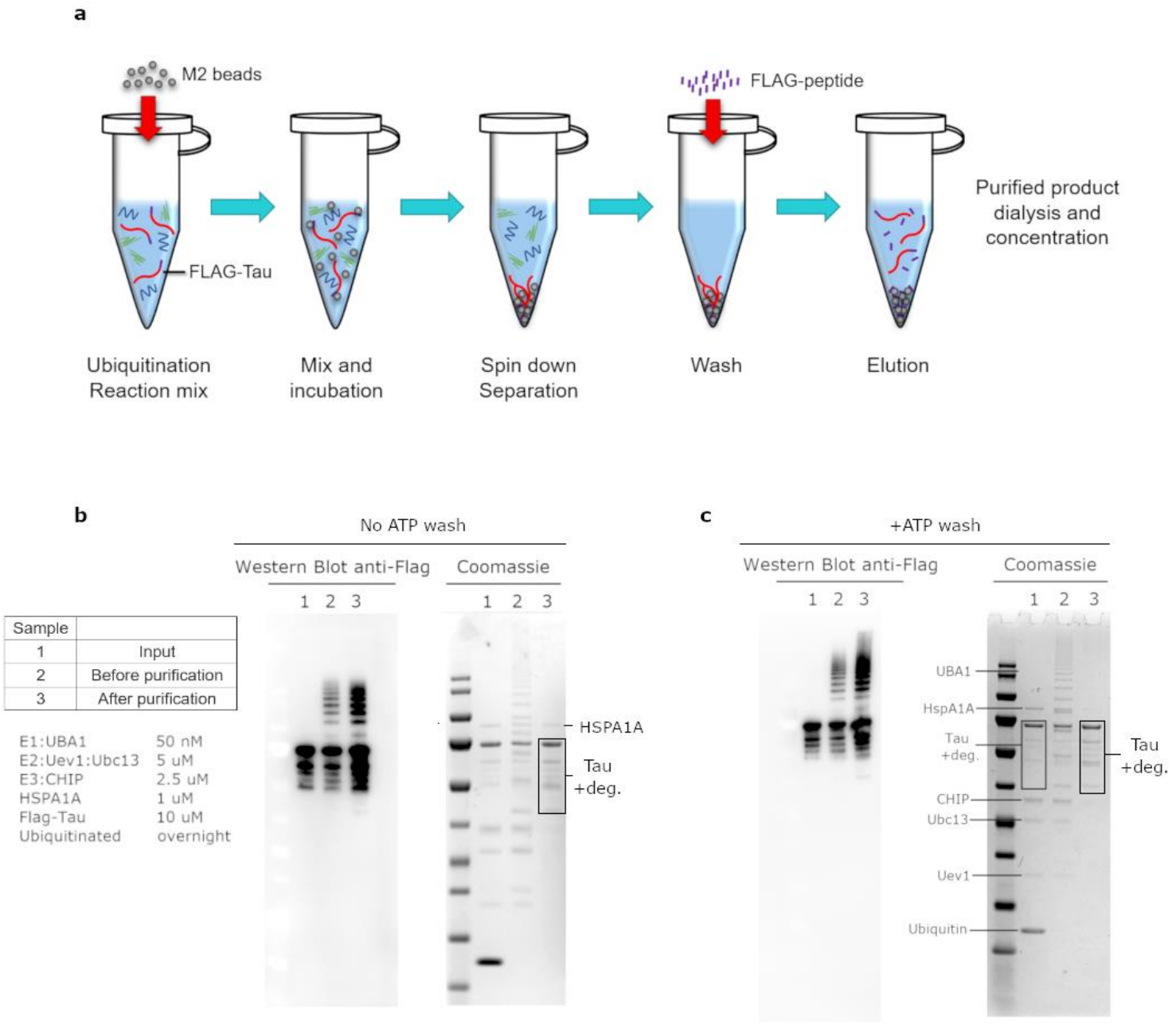

Figure 6: purification of ubiquitinated Tau from the ubiquitination machinery mix.

(a) Schematic illustration of Tau purification by anti-FLAG M2 affinity gel beads. M2 beads were added to the ubiquitination reaction mix and the bait reaction was incubated for 1 hour. Tau proteins were separated by centrifugation, while other components were washed away. The elution of Tau from M2 beads is conducted by FLAG peptide addition.

(b) Anti-FLAG (Tau) western blot and SDS-PAGE gel of Tau purification without ATP wash.

(c) Anti-FLAG (Tau) western blot and SDS-PAGE gel of Tau purification plus ATP wash.

Condensate formation of ubiquitinated Tau with autophagy cargo receptors p62 and NBR1

After succeeding in enriching ubiquitinated Tau, I next tested its interaction with-and potential condensate formation by the cargo receptors p62 and NBR1. I used the mCherry tagged version of p62 with a point mutation S403E, which mimics the phosphorylation at serine 403 that mediates stronger ubiquitin binding[21], NBR1 was EGFP tagged. The proteins were mixed directly in a 384 wells plate and the condensates were observed with a spinning disc microscope after 4 hours incubation at room temperature.

First, I tested Tau ubiquitinated with K63-linked chains generated by Uev1:Ubc13 and CHIP/HSPA1A (Figure 7a). When p62 was added to ubiquitinated Tau, formation of only a few condensates was observed. Adding NBR1 alone to ubiquitinated Tau had yielded a similar result. However, adding p62 and NBR1 simultaneously to ubiquitinated Tau dramatically boosted the number of condensates formed (See also Figure 7e, enlargement of 7a for better distinguishment). The condensates observed by mCherry-p62 S403E and EGFP-NBR1 were shown to colocalize together after merging, suggesting strongly that both of the two cargo receptors can recognize ubiquitinated Tau as cargo, and the presence of both greatly enhances the recruitment to the cargo mutually.

I then verified that the condensate formation is induced by Tau ubiquitination using Tau incubated with the ubiquitination machinery without ATP and again purified Tau via anti-FLAG beads. Tau remained non ubiquitinated as confirmed by western blot (Figure 7g), and adding p62 and NBR1 did not result in condensation formation (Figure 7a, 5th panel. Figure 7f, enlargement of 7a for better distinguishment).

The other E2/E3 combinations that mainly attach K48-linked and mixed chain types were also tested in the same experimental settings. The two combinations used UbcH5B as E2, and either MARCHF7 RING domain or CHIP/HSPA1A as E3 (Figure 7b and c, respectively). Both of these two combinations also showed ubiquitination dependent condensate formation. The numbers and area of the condensates induced by Tau ubiquitination were quantified using an ImageJ plugin (Figure 7d). No concrete conclusions could be given regarding the amount and area of the condensates generated by different ubiquitin chain types, likely due to the difficulties in quantifying the exact amount of Tau used as input and intrinsic variation in chain lengths and types. Thus, no statistical analysis was performed for the quantification. Nevertheless, the observation that ubiquitinated Tau can induce condensate formation with autophagy cargo receptors p62 and NBR1 strongly suggests that Tau can be specifically recognized as cargo for selective autophagy degradation, and that this recognition is

ubiquitination dependent. Furthermore, the presence of both p62 and NBR1 synergistically enhances the recruitment of each other to ubiquitinated Tau.

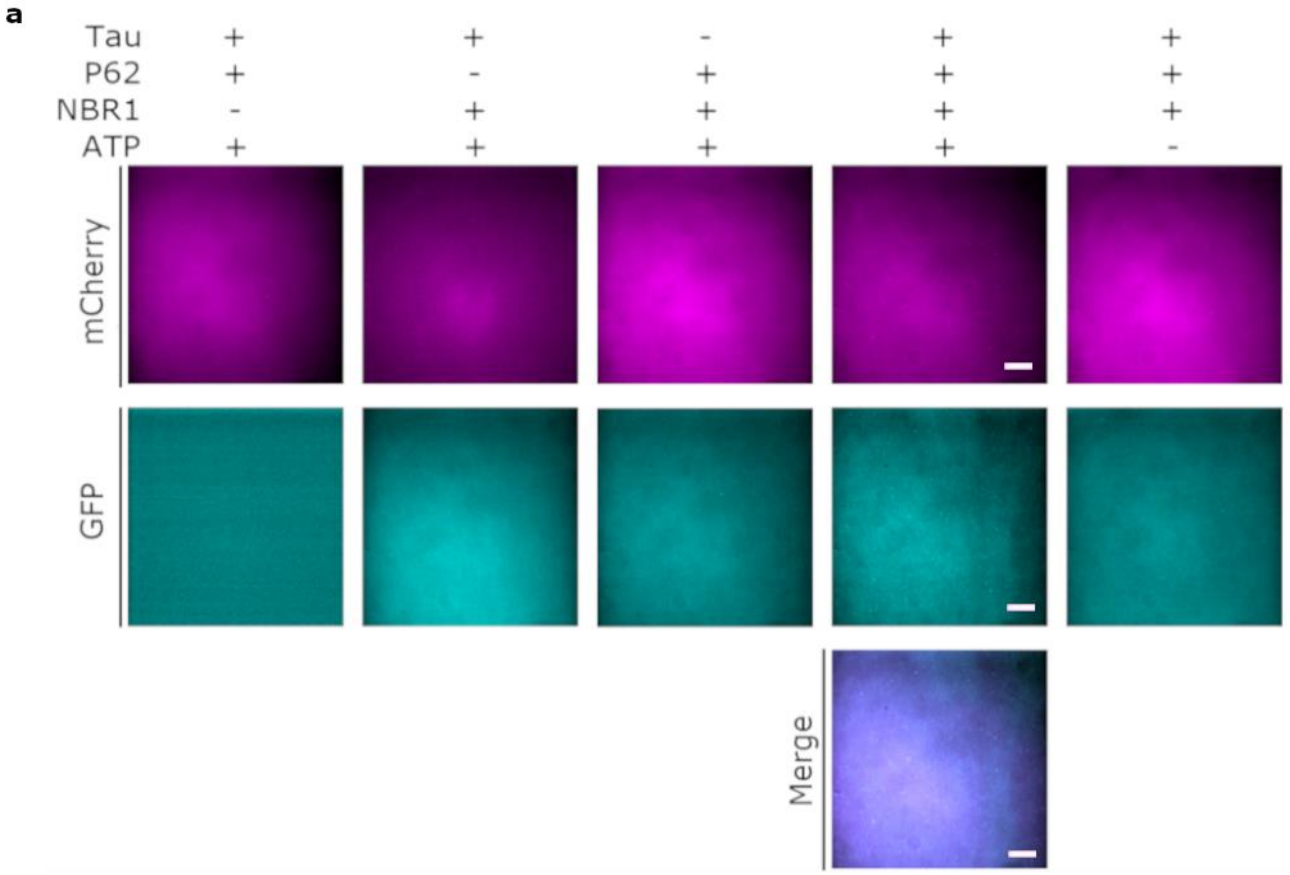

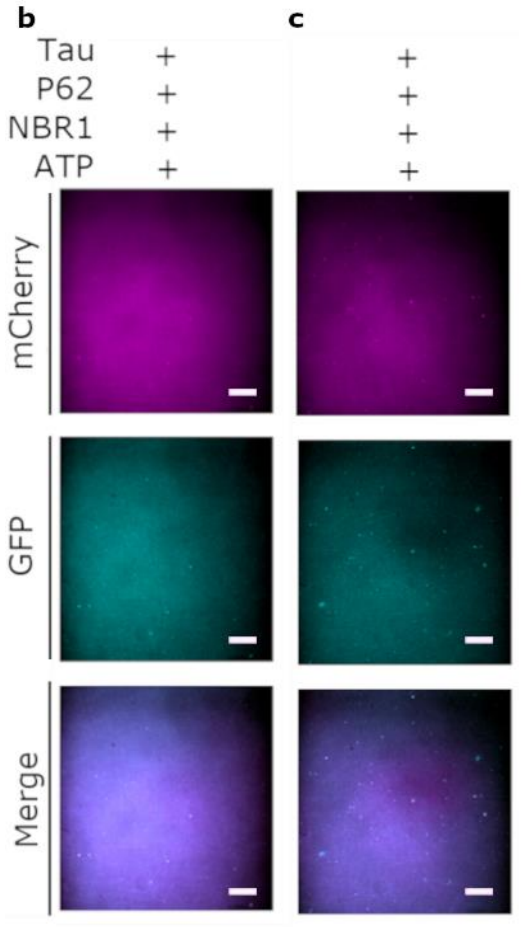

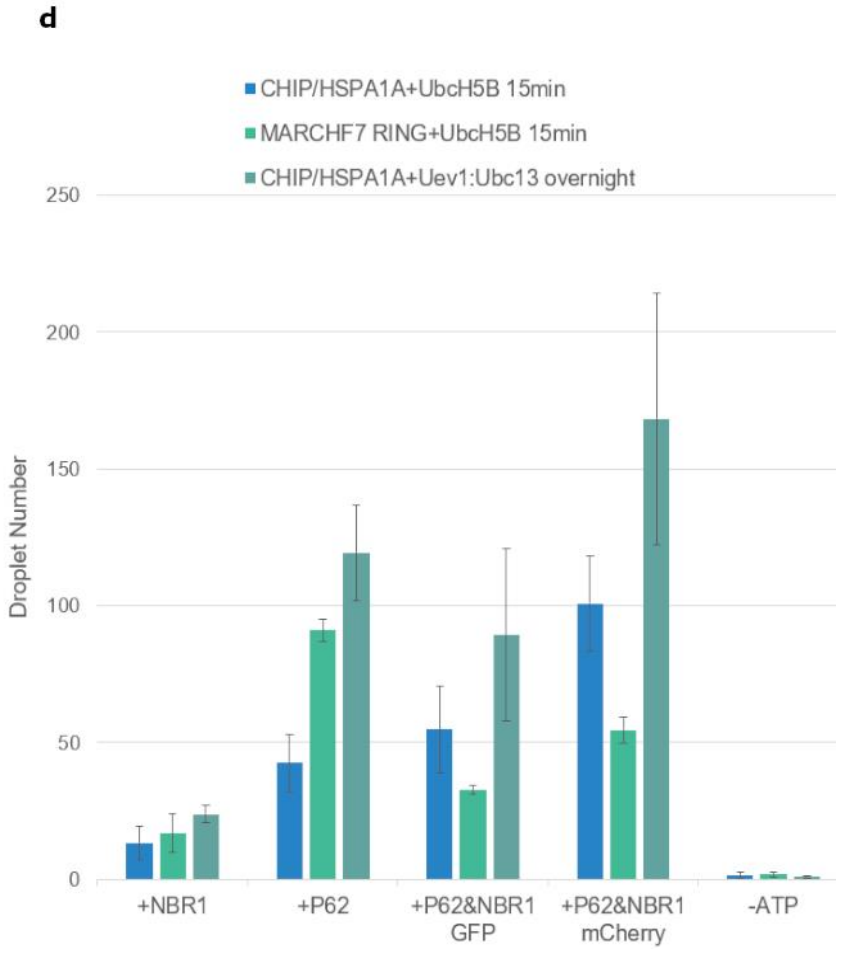

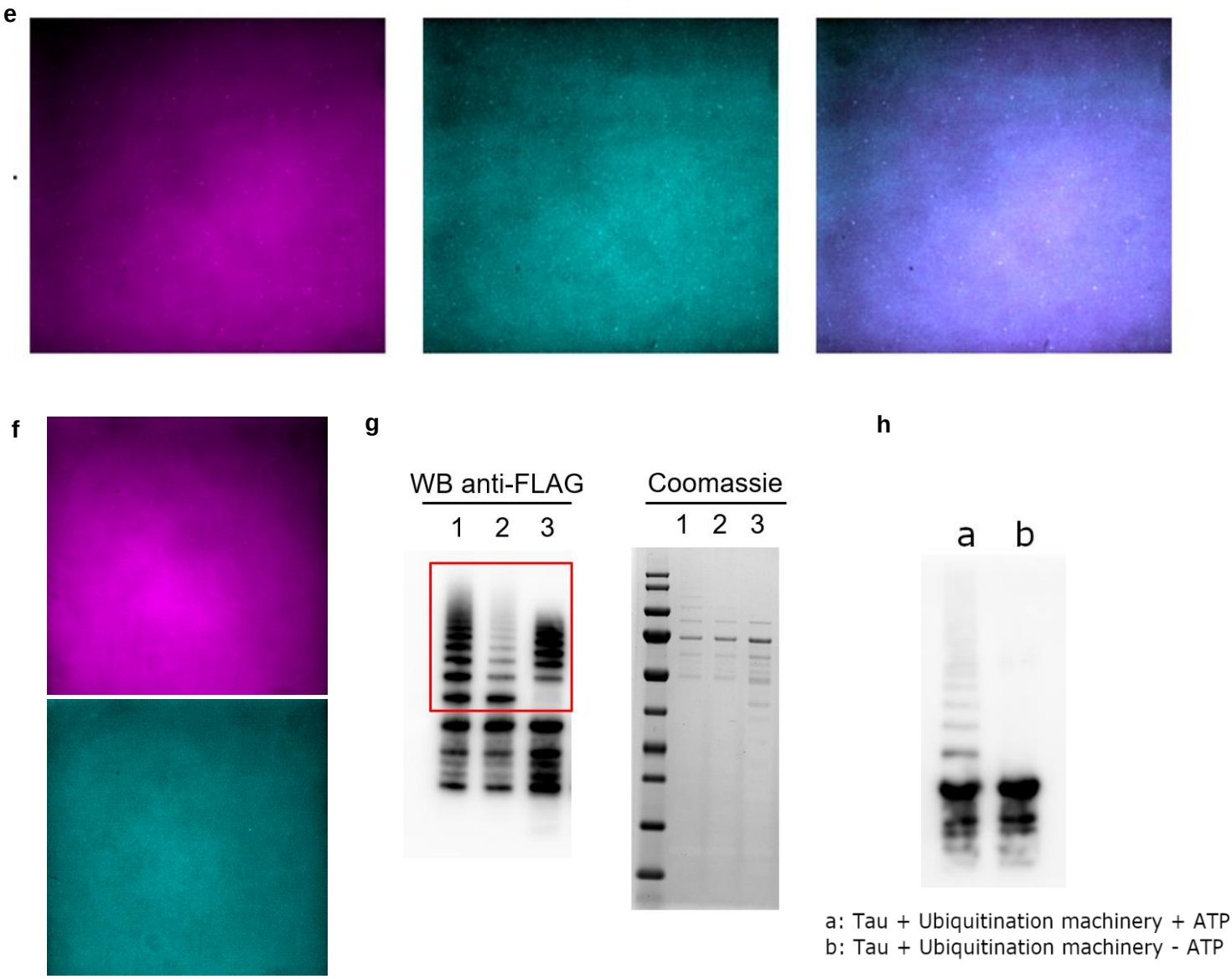

Figure 7: Condensate formation of ubiquitinated Tau with autophagy cargo receptors p62 and NBR1

(a) Ubiquitinated Tau condensate formation by p62 and NBR1 assessed by spinning disk microscopy after 4 hours incubation. Red (mCherry-p62, in magenta) and green (EGFP-NBR1 in cyan) channels are shown. Scale bars 10 µm.
(b) As in (a), but using UbcH5B as E2 and CHIP/HSPA1A as E3. Scale bars 10 µm
(c) As in (a), but using UbcH5B as E2 and MARCHF7 RING domain as E3. Scale bars 10 µm
(d) Quantification of condensates. Error bars showing standard deviation with n=3.
(e) Enlargement of (a), 4th panel.
(f) Enlargement of (a), 5th panel.
(g) Western blot and SDS-PAGE gel of different inputs of ubiquitinated Tau for concentration comparison.
(h) Western blot of Tau ubiquitinated with or without ATP after M2 beads purification.

Tau colocalization with p62 and NBR1 in condensates

Since data suggested that condensate formation is induced by ubiquitinated Tau, I wanted to further verify that Tau is indeed colocalizing in the condensates together with the fluorescently tagged cargo receptors p62 and NBR1 (Figure 8a). As I used mCherry-p62 and EGFP-NBR1, a third fluorophore was needed to distinguish the presence of Tau in the condensates. Tau protein is FLAG tagged, therefore the mouse anti-FLAG M2 antibody that specifically recognizes FLAG-Tau was used in dilution series to recognize Tau in the condensates. The Alexa Fluor 405 goat anti-mouse secondary antibody was used to allow detection by microscopy. The colocalization of the three fluorophores was observed via confocal microscopy.

The ubiquitinated Tau was purified from the ubiquitination components and incubated with p62 and NBR1 for 4 hours to form condensates. After that, primary mouse anti-FLAG antibody was added into the mix in different dilutions 1:200, 1:500 and 1:2000 (where 1:200 is normally used in western blot) and incubated overnight at 4°C. The Alexa Fluor 405 goat anti-mouse secondary antibody was then added at a concentration of 1:500 (where 1:250 is recommended for immuno-fluorescence) and after 1 hour of incubation at room temperature, the colocalization of the three fluorophores was determined for condensates which sedimented to the bottom of the wells. I focused on the sedimented condensates, as the floating ones in suspension were hard to capture by the confocal microscope due to their fast movement. As a negative control, the Alexa Fluor 405 goat anti-mouse secondary antibody was added to the condensation reaction without addition of the primary anti-FLAG antibody. Replacement of ubiquitinated Tau with artificial cargo GST-tetra-ubiquitin (GST-4xUb) or buffer were used as further negative controls. (Figure 8b, c)

Considerable overlap of the fluorescence pattern for the three fluorophores could be observed when p62, NBR1 and FLAG-Tau were present and incubated with the anti-FLAG antibody, which strongly suggested that the Tau protein is present in the condensates. The concentration of the primary antibody added in to the condensation mix had no significant effect on the recognition of Tau, whereas removing the primary anti-FLAG antibody and adding only the Alexa Fluor 405 secondary antibody completely abolished the colocalization of anti-Tau signal with the cargo receptors, indicating that the secondary Alexa Fluor 405 secondary antibody does not simply stick to p62-NBR1 aggregates. The absence of Tau and replacement of Tau with GST 4xUb further ascertained the specificity of the assay, as the colocalization of the three fluorophores in these two negative controls were observed only sporadically, and was markedly lower compared to the full reaction.

To sum up, I have established an effective and reliable method for detecting the presence of Tau in the condensates formed by fluorescently tagged cargo receptors. The Tau protein is shown to be colocalizing in the condensates with p62 and NBR1, which showed that Tau could indeed be recognized and clustered by autophagy cargo receptors.

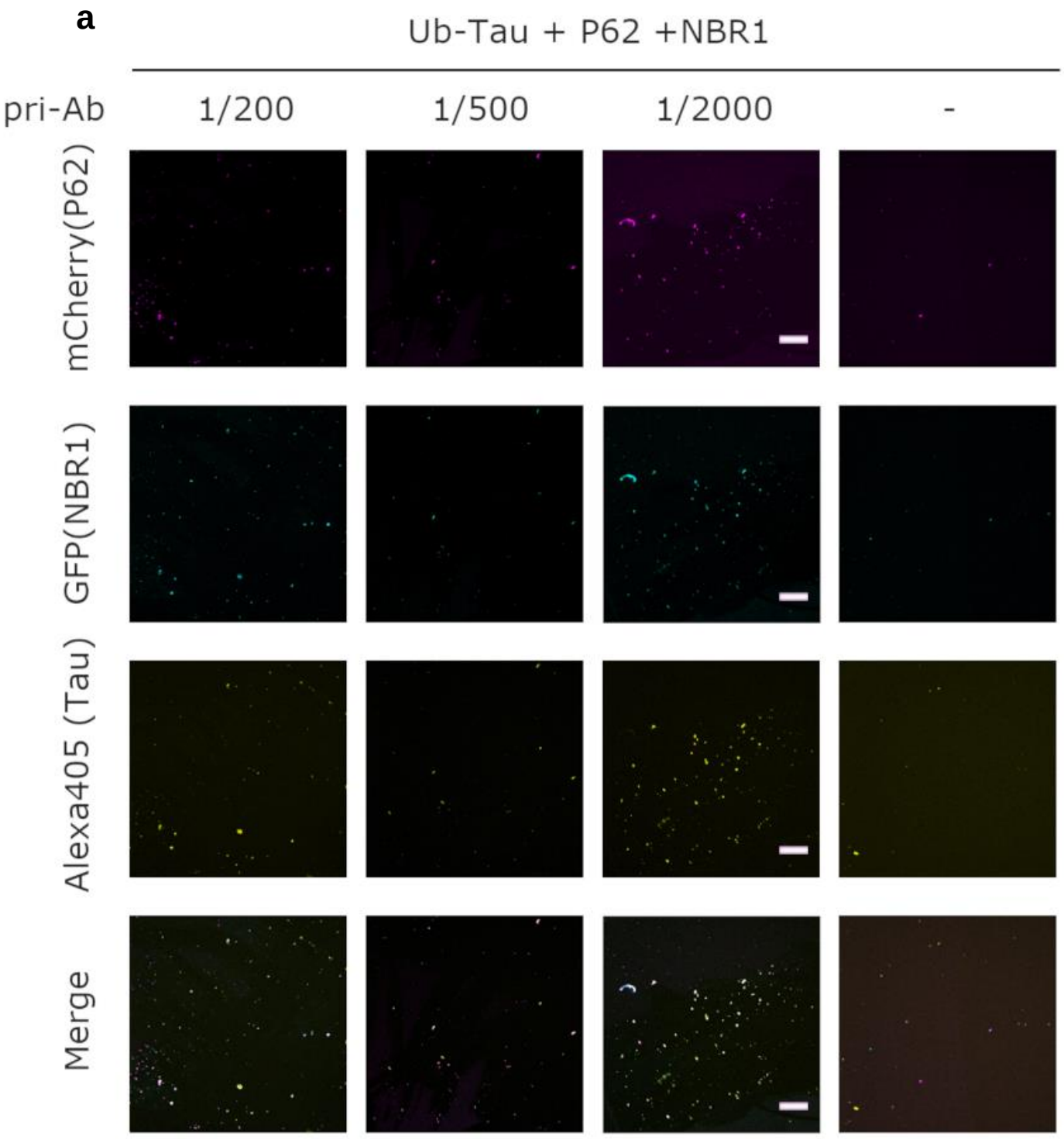

Figure 8: Antibody staining showing Tau colocalization with p62 and NBR1 in condensates.

Primary antibody mouse anti-FLAG.

Secondary antibody Alexa Fluor 405 goat anti-mouse. (1:500)

(a) Ubiquitinated Tau (blue channel, in yellow) co-localization with mCherry-p62, (red channel, in magenta) and EGFP-NBR1 (green channel, in cyan) assessed by confocal microscopy.

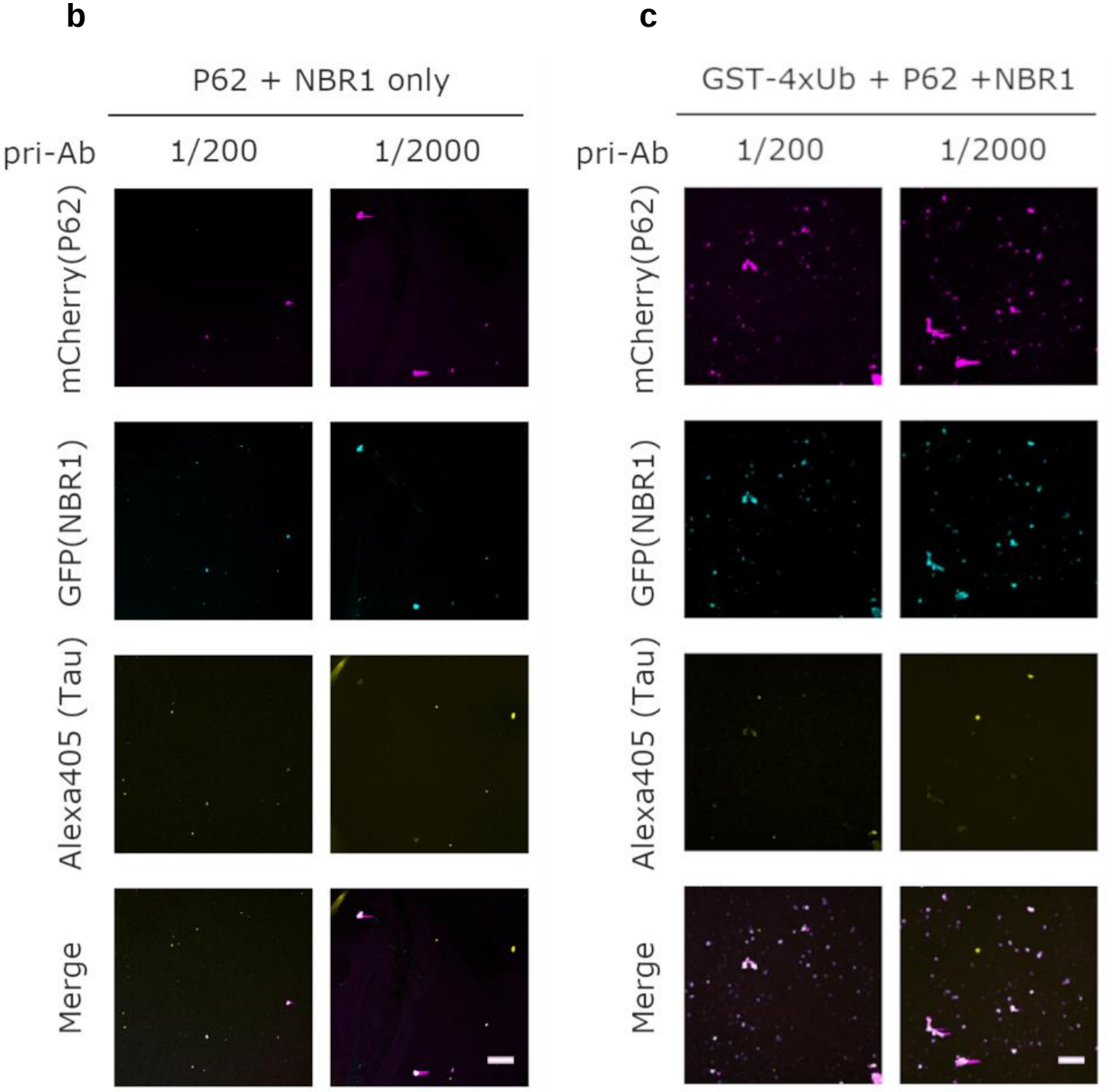
b
P62 + NBR1 only
pri-Ab
1/200
1/2000
mCherry(P62)
GFP(NBR1)
Alexa405 (Tau)
Merge
c
GST-4xUb + P62 +NBR1
pri-Ab
1/200
1/2000
mCherry(P62)
GFP(NBR1)
Alexa405 (Tau)
Merge

Kinetics of condensate formation

Next, I investigated the kinetics of condensate formation. Purified K63 chain ubiquitinated Tau protein was pipetted into a buffer solution containing mCherry-p62 and EGFP-NBR1, and images were taken via spinning disc microscopy immediately after the solution was mixed and the plate was sealed with parafilm to reduce evaporation. Condensates were observed in both mCherry and GFP channels, and pictures were taken every 2-10 minutes intervals to avoid bleaching of the fluorophores. The total duration of recording lasted 8 hours to capture the maximum increase of the condensate number and total area (the figures show acquisitions only up to 5 hours, as the condensate numbers and the total area were constant afterwards). The mCherry signal was stronger and more distinct than the EGFP one. Therefore, the pictures of the mCherry channel were used for quantification. Figures were quantified using ImageJ as described in the Methods section.

The condensate numbers and total area kept increasing over time (Figure 9a). The mCherry-p62 showed stronger signal than NBR1, consistent with the former static observations described above. The condensates were dynamic and moved freely in the solution. A mix of p62 and NBR1 without addition of Tau was used as negative control, and almost no condensates were observed in both fluorescence channels throughout the recording. When compared to the positive control deploying GST-4xUb instead of ubiquitinated Tau, condensates were less in number and smaller in size.

Quantification of the condensate numbers and total area was performed via ImageJ, with both parameters showing kinetics (Figure 9b, c). The proportional increase of the condensate number and total area of condensates indicated that the size of the condensates maintained within a relative stable range. The quantification revealed growth curve that reached a plateau at around 240 minutes. The condensate number and total area was calculated by addition of numbers of the condensates from 5 planes of a z-stack for each time point to minimize the occasional fluctuation, and stabilized at around 200 condensates per field. In comparison, GST-4xUb rapidly forms more condensates larger in area, and plateaued in a relative short time of around 60 minutes. The slower kinetics of Tau-induced condensate formation could be either be due to the lower concentration, or due to the structural differences compared to GST-4xUb. Indeed, the Tau protein is ubiquitinated with different ubiquitin chain length which are attached to various lysine residues on Tau, whereas the dimeric GST-4xUb has a homogeneous chain length of 4 units. Furthermore, the calculated concentration of Tau considers total Tau including non-ubiquitinated populations, implying that the actual concentration of ubiquitinated Tau is much lower than the apparent 5 µM. Thus, having a

higher concentration of ubiquitinated Tau protein in the solution mix could potentially boost the condensate formation and display kinetics similar to GST-4xUb. To this end, further optimization of Tau ubiquitination patterns (chain type, length and targeted lysine) is likely to result in different condensation kinetics.

In conclusion, I showed that the number and total area of condensates induced by p62 and NBR1 recognition of ubiquitinated Tau increase proportionally over time, suggesting that the size of the condensates maintained within a relative stable range. The kinetics of condensate formation revealed a growth curve that reached stationary phase at around 240 minutes and stabilized afterwards.

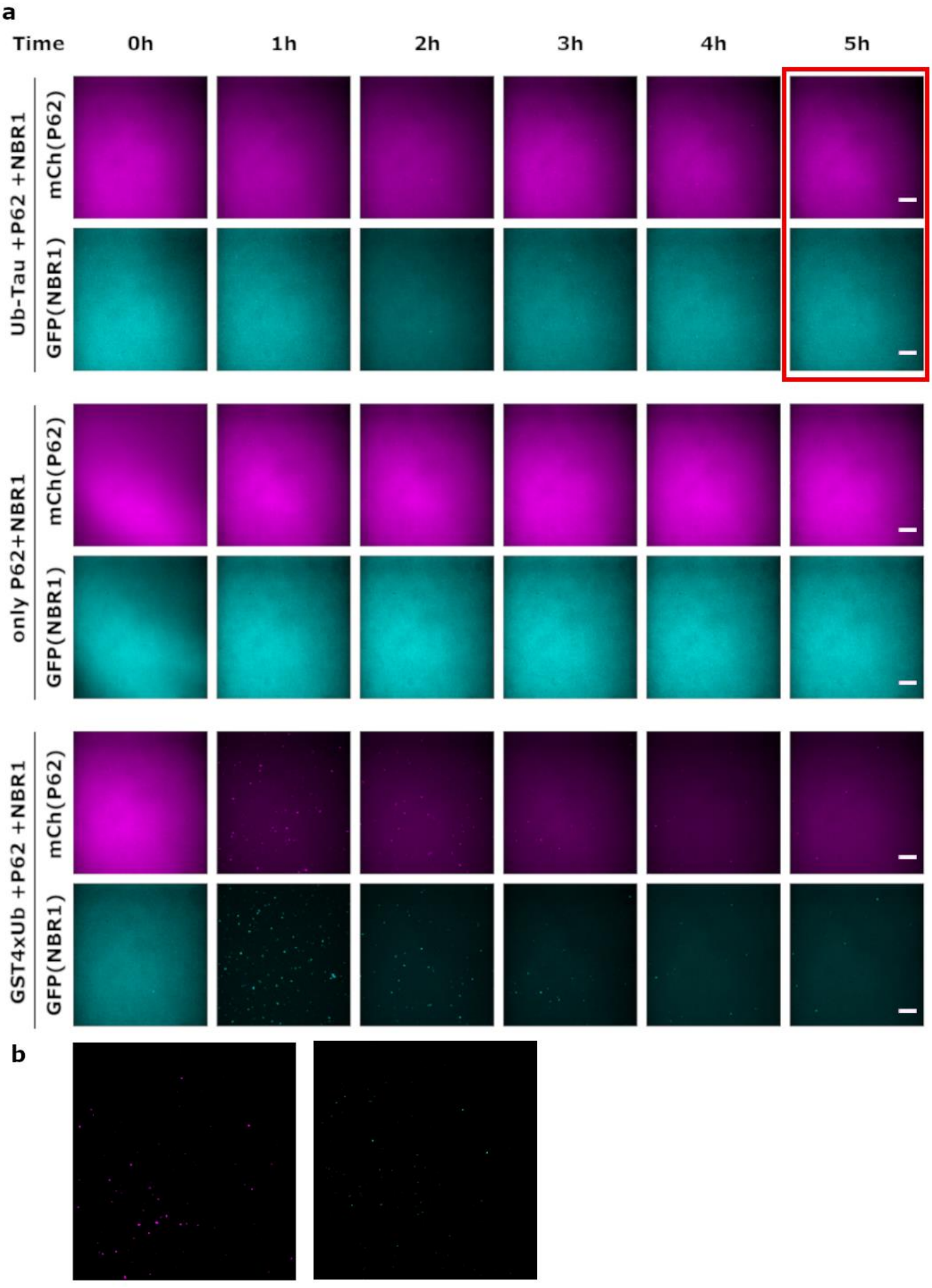
a
Time
0h
1h
2h
3h
4h
5h
Ub-Tau +P62 +NBR1
mCh(P62)
GFP(NBR1)
only P62+NBR1
mCh(P62)
GFP(NBR1)
GST4xUb +P62 +NBR1
mCh(P62)
GFP(NBR1)
b

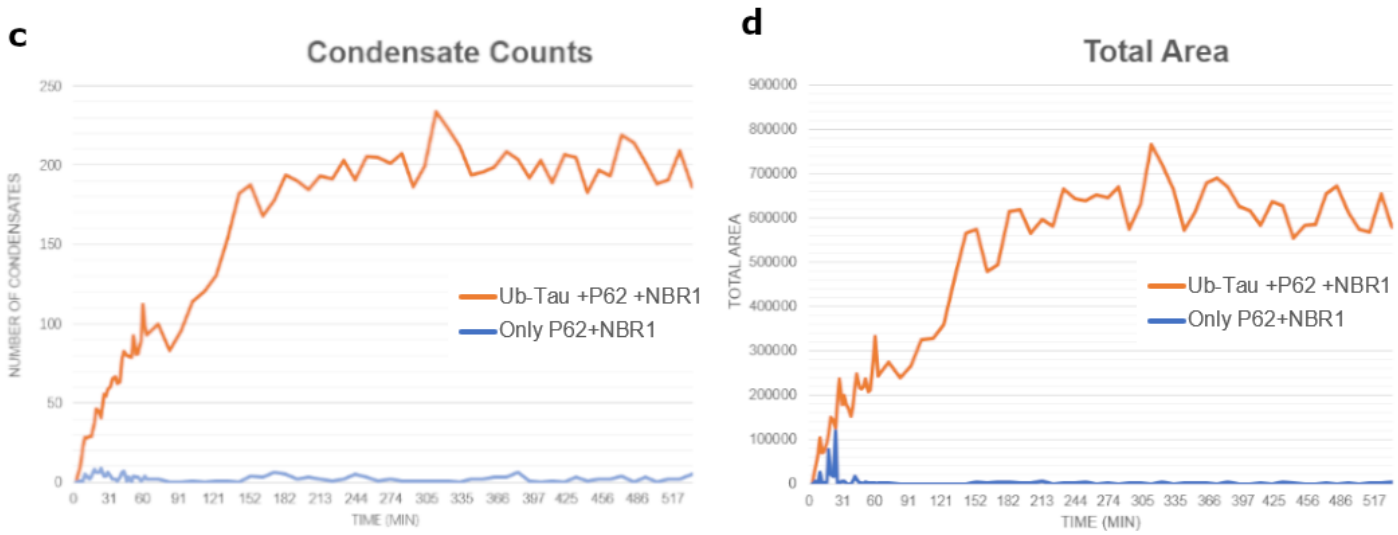

Figure 9: Kinetics of condensate formation induced by ubiquitinated Tau recognition by the cargo receptors p62 and NBR1.

(a) Condensate formation by p62 and NBR1 assessed by spinning disk microscopy, in the presence of ubiquitinated Tau (bottom panel), buffer (middle panel) or GST-4xUb (lower panel). Red (mCherry-p62, in magenta) and green (EGFP-NBR1 in cyan) channels are shown. Scale bars 10 µm.

(b) Binarized figure of Tau condensate formation with p62 and NBR1, figure 9 (a) red box.

(c) Quantification of condensate numbers in the presence or absence of ubiquitinated Tau.

(d) Quantification of condensate total area (number of pixels) in the presence or absence of ubiquitinated Tau.

Effects of truncated cargo receptors p62 and NBR1 on condensate formation

In order to have a deeper understanding of how the cargo receptors recognize ubiquitinated Tau as autophagy cargo, I used different truncations of p62 or NBR1, respectively in combination with full length EGFP-NBR1 or mCherry-p62 S403E (Figure 2). Two truncated versions of p62 were employed: mCherry-p62-ΔPB1 (Δ2-102) and mCherry-p62-ΔUBA (Δ389-431). The N-terminal PB1 domain of p62 mediates self-oligomerization and serves as an interaction interface for other PB1-containing proteins to form oligomers[62], while the UBA domain allows p62 to associate with ubiquitin and thus to recognize ubiquitinated cargo proteins and form cytosolic aggregates[63]. For NBR1, I used the EGFP-C-terminal half of NBR1 (499-966) which contains the UBA domain but not the PB1 domain, and EGFP-NBR1-ΔUBA (Δ913-957). Similar to p62, The PB1 domain of NBR1 is responsible for interaction with p62, whereas the UBA domain recognizes and associates with ubiquitinated cargos.

In consistence with our former observation, p62 S403E and WT NBR1 alone could form few condensates with ubiquitinated Tau, and the presence of both cargo receptors greatly promoted the condensation, increasing the number of the condensates (Figure 10, top rows on upper and lower panels; quantifications in Fig 10c and 10d). When I replaced the mCherry-p62 S403E with mCherry-p62-ΔPB1, no visible condensates were observed in the red channel (Figure 10a, second row on upper panel). Few condensates could be seen in the green channel, consistent with EGFP-NBR1 capable of forming by itself condensates with ubiquitinated Tau. The deletion of the PB1 domain abolishes the self-oligomerization of p62 and its interaction with NBR1[23], in turn diminishing the condensation of cargo receptors with ubiquitinated Tau. Similarly, having mCherry-p62-ΔUBA instead of mCherry-p62 S403E also impaired condensate formation (Figure 10a, third row on upper panel), which is very likely to be caused by the inability of truncated p62 to recognize and associate with ubiquitinated Tau. The replacement of EGFP-NBR1 with a truncation containing only the C-terminal half of NBR1 (K499-Y966) also demonstrated the importance of the PB1 domain containing N-terminal half in the condensate formation (Figure 10a, second row on lower panel). In these conditions, only few condensates were observed in the mCherry channel by p62 S403E and these condensates did not overlap with condensates in the GFP channel formed by EGFP-NBR1. Unexpectedly, using EGFP-NBR1-ΔUBA instead of the full length NBR1 showed comparable numbers of condensates (Figure 10a, third row on lower panel). The number of condensates in the mCherry channel is reduced by half and now comparable with the condensate numbers in the GFP channel, in contrast with complete abolishment of

condensate formation observed in both channels when p62 was replaced with p62-ΔUBA. The deletion of UBA domain from NBR1 impair its ubiquitin association and should thus abolish the condensate formation with Tau. This indicates that p62 UBA domain could partially rescue the function of NBR1 UBA domain.

Overall, truncated cargo receptors lacking either the PB1 domain or the UBA domain form reduced number of condensates, indicating that both the ubiquitin binding function and self-oligomerization property are essential for the cargo recognition and aggregation for further autophagy degradation.

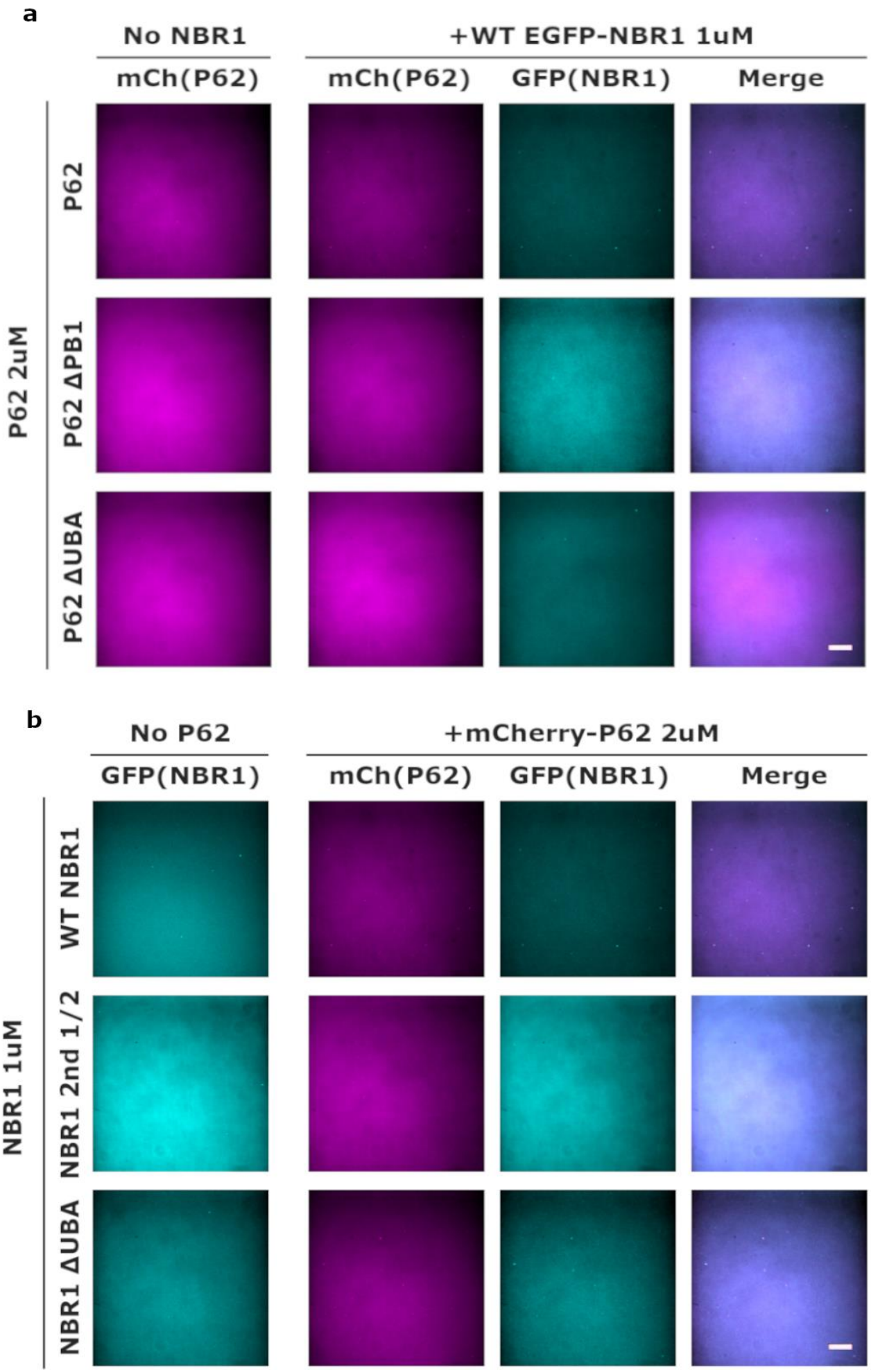
a
No NBR1
+WT EGFP-NBR1 1uM
mCh(P62)
mCh(P62)
GFP(NBR1)
Merge
P62 2uM
P62
P62 ΔPB1
P62 ΔUBA
b
No P62
+mCherry-P62 2uM
GFP(NBR1)
mCh(P62)
GFP(NBR1)
Merge
NBR1 1uM
WT NBR1
NBR1 2nd 1/2
NBR1 ΔUBA

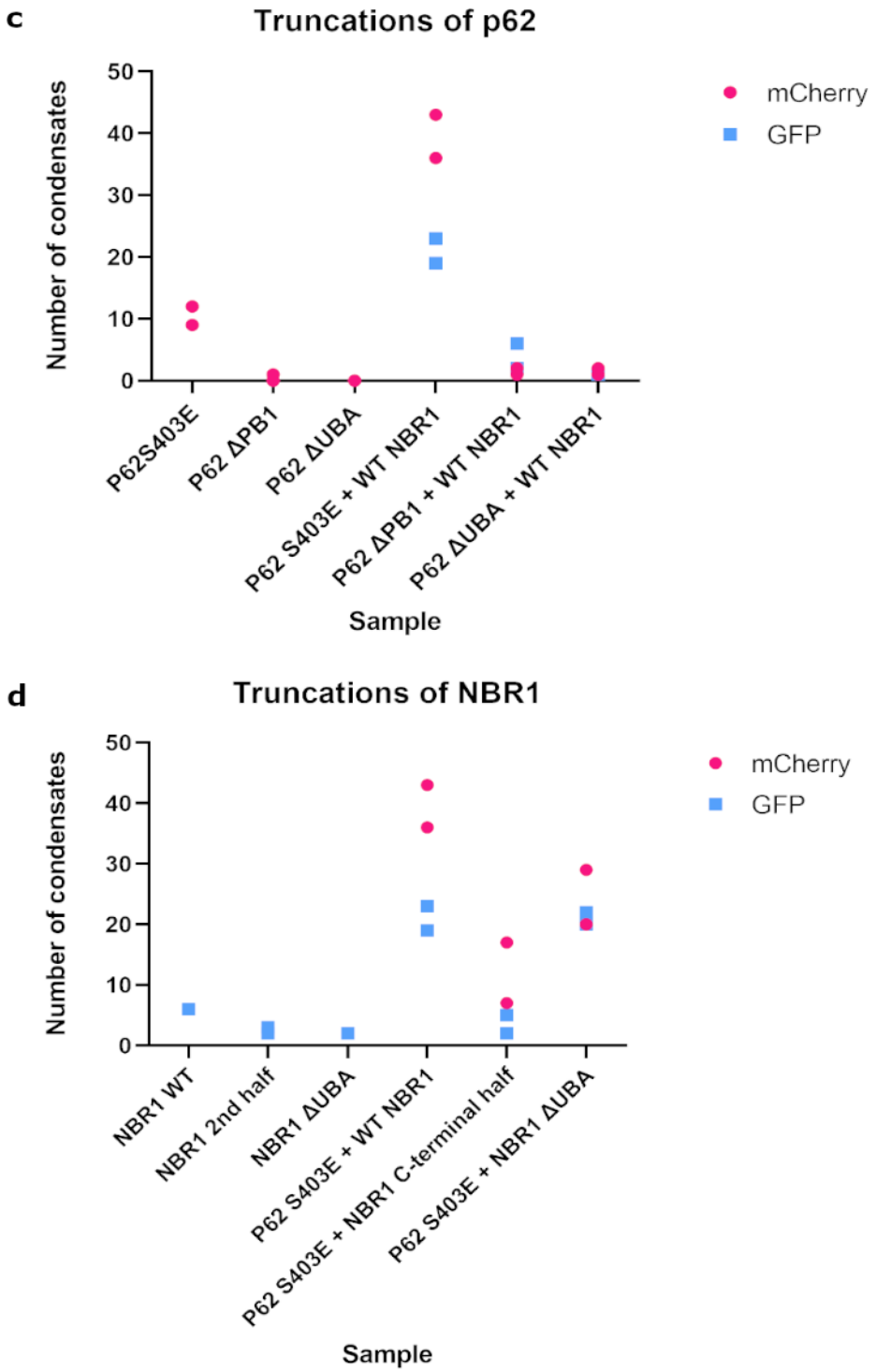

Figure 10: The effect of truncated cargo receptors p62 and NBR1 on the condensate formation with ubiquitinated tau. The deletion of either the PB1 domain or the UBA domain from p62 and NBR1 resulted in overall reduction in the number of condensates. Condensate formation by different truncations of p62 and NBR1 assessed by spinning disk microscopy in the presence of ubiquitinated Tau after 4 hours. Red (mCherry-p62, in magenta) and green (EGFP-NBR1 in cyan) channels are shown.

(a) Condensate formation with ubiquitinated tau by p62 and p62-ΔPB1 and p62-ΔUBA.
(b) Condensate formation with ubiquitinated tau by WT NBR1 and the EGFP-C-terminal half of NBR1 and NBR1-ΔUBA.
(c) Quantification of condensate numbers of (a), data of 2 replicates.
(d) Quantification of condensate numbers of (b), data of 2 replicates.

Discussion

In this work, I characterize different ubiquitination patterns on Tau protein by either using as E3s MARCHF7 or by using CHIP in combination with HSPA1A, known to adopt a bipartite Interaction to ubiquitinate substrates[64]. I used two different E2s: UbcH5B and Uev1:Ubc13. Ubiquitination plays an important role in Tau homeostasis and it was proposed that site-specific ubiquitination of Tau can influence the filament structure and mediate fibril subpopulations in Alzheimer's disease[65]. Among the combinations tested, CHIP/HSPA1A and Uev1:Ubc13 worked together and attached mainly K63-linked chains to the Tau which has been generally considered as a signature for autophagy degradation rather than proteasome degradation[28,29]. When compared to the rapid ubiquitin chains synthesis by other E2 and E3 combinations that attached mainly K48-linked chains, the low ubiquitination efficiency and long assembling time are in consistence with the role of autophagy to degrade long-lived proteins and insoluble protein aggregates[9], suggesting that the autophagy pathway of Tau degradation might serve as a backup plan, which will only act to compensate the degradation of the monomeric or aggregated forms of Tau when they are not removed in a timely manner by the ubiquitin-proteasome system. CHIP expression has been observed in AD brain tissues with Tau accumulation[66], and Tau ubiquitination by this E3 should be the focus of further research.

After Tau ubiquitination, I established a reproducible protocol for purifying Tau protein (ubiquitinated and monomeric as well) from the ubiquitination machinery with high efficiency and purity, using the M2 anti-FLAG beads.

So far, experiments reconstituting cargo recognition and phase separation by autophagy cargo receptors in vitro have been done with mainly artificial cargos (e.g., GST-4xUb) with homogenous ubiquitin chain length and same patterns on lysine residues[23,25,67]. In this work, I expanded to physiological relevant cargo to study the recognition of ubiquitinated Tau by autophagy cargo receptors. I took the purified ubiquitinated Tau and mixed it with cargo receptors p62 and NBR1 in solution, to observe the clustering of cargo receptors p62 and NBR1 with ubiquitinated Tau, and whether they could recognize ubiquitinated Tau as cargo and if such recognition and interaction would induce condensate formation for autophagy degradation. I demonstrated that the condensate formation of Tau with autophagy cargo receptor p62 and/or NBR1 is ubiquitination dependent, consistent with previous description with artificial cargoes[25]. The presence of both p62 and NBR1 was shown to mutually promote the condensate formation of Tau significantly.

I also compared the condensate formation with Tau ubiquitinated by different combinations of E2s and E3s. Even though I could not make any concrete conclusions on the difference between condensate formation induced by different ubiquitin chain types due to lack of replicants, I could speculate that K48-linked or mixed chain ubiquitinated Tau could be more soluble and efficiently recognized by various cargo receptors and shipped to be degraded by the UPS pathway, while K63-linked Tau might possess a higher propensity for aggregation and less accessibility for cargo receptors, which will only be gradually degraded by the autophagy pathway. Further experiments are needed to verify this hypothesis.

Testing different truncations of p62 and NBR1 allowed us to dissect their contribution to condensate formation. For p62 I used p62-ΔPB1 and p62-ΔUBA and for NBR1, I took the EGFP-C-terminal half of NBR1 (PB1 domain not present) and NBR1-ΔUBA. The results are generally in line with our understanding of domains on the cargo receptors. PB1 is known to be responsible for self-oligomerization and interacts with PB1 domains on other proteins to form heterooligomers[26,62]. The deletion of PB1 in either cargo receptor abolished the robust condensate formation by p62 S403E and WT NBR1, assembling the level of condensate numbers when only one cargo receptor is present. The UBA domain that associate with ubiquitin and facilitates the binding with ubiquitinated cargos[20,63] was shown to be essential for the condensate formation in the case of p62. However, when I tested the NBR1-ΔUBA, the condensate formation was only weakened but not completely abolished. I therefore speculate that the function of NBR1 UBA domain could be rescued partially by the p62 UBA domain.

Based on previous researches and on my observations, I proposed a working model. The Tau protein is ubiquitinated in vivo by different combinations of E2s and E3s, a process that is likely partly determined by other post-translational modifications on Tau. A variety of ubiquitin chain types on different lysine residues are attached to the Tau protein. DUBs may also play an important role in this process by reversing the ubiquitination thus avoiding Tau degradation. The ubiquitinated Tau with K48-linked or mixed ubiquitin chain types might be synthesized more efficiently which will then lead to the choice of proteasome degradation pathway. On the other hand, the K63-linked ubiquitinated Tau might be more prone to aggregation and adopting a conformation that is less accessible to the cargo receptors. However, once the condensate is formed, the Tau protein may be bulkily degraded through the autophagy pathway. While p62 primarily drives the recognition of ubiquitinated Tau, NBR1 interacts with p62 and further promotes clustering and condensate formation. Together they recruit other components of the autophagy machinery, such as TAX1BP1 and

FIP200[68,69]. This bridges the condensates to the isolation membrane and the cargo Tau protein will be degraded.

This work employed monomeric Tau for a bottom-up reconstitution of Tau ubiquitination and recognition. Nonpathological protein was studied, but established protocols can already be applied to pathological Tau fibrils. Our research on the Tau protein can be expanded from physiological autophagy degradation under normal condition to disease related alterations in Tau clearance.

Further research could be planned from several aspects. A better understanding of ubiquitinated Tau chemistry (chain length, ubiquitin type, lysine residues targeted) will allow us to compare the formation of condensates induced. Another Tau specific E3 TRAF6[58] can be investigated in the same assay, and I have already cloned full length TRAF6, the expression and purification of which needed further optimization. Since p62 has been found to bind TRAF6 and TRAF6 is also found in the inclusion bodies isolated from AD brains, the participation of TRAF6 might give exciting results. In addition, more cargo receptors and components of ubiquitination machinery could be added upon the condensate formation. Addition of TAX1BP1 and FIP200 may further promote the condensate formation and provide us with a deeper insight into the shipment of the Tau protein to the autophagosome. Furthermore, molecular chaperones have been shown to cooperate with the aggrephagy machinery by binding to protein aggregates as well as p62 to promote cargo clearance via autophagy[70]. Thus, it could be investigated whether addition of relevant chaperones to the condensation assay could further increase p62 clustering with ubiquitinated Tau could be investigated. Another direction by adding DUBs and several Tau specific DUBs have been so far identified[71,72]. The ability of DUBs to deubiquitinate ubiquitinated Tau can be checked on western blot and by adding DUBs into the solution while condensates are formed. Finally, as Tau hyperphosphorylation has been linked in several studies to neurodegenerative diseases[73–75], phosphorylated or pseudo-phosphorylated Tau could be reconstituted and ubiquitinated and added to the condensation assay. Correlation between PTMs and different regions or isoforms of Tau in a cohort of AD patients have also been discussed[76], studying their effect on condensate formation could be valuable to understand the pathological role played by Tau PTMs. Finally, the assays I developed could be translated to other neurodegenerative diseases.

This thesis establishes a starting point for the in vitro investigation of Tau ubiquitination and its autophagic degradation. Methods and protocols that could be particularly useful for further studies were established and can be followed and replicated. More open questions are still

to be answered, and our in vitro study may eventually result in concrete prediction, which can be tested *in vivo*.

Abbreviations

UPS	Ubiquitin-proteasome system
PB1	Phox and Bem1
UBA	Ubiquitin association
p62 S403E	p62 serine 403 to glutamate
DUBs	Deubiquitinases
AD	Alzheimer’s disease
MAPT	Microtubule-associated protein Tau
NFT	Neurofibrillary tangles
WT	Wild type
GOI	Gene of interest
IPTG	Isopropylthiogalactoside
Amp	Ampicillin
CAM	Chloramphenicol
ROI	Region of interest

Acknowledgment

First and foremost, I want to thank my supervisor Dr. Sascha Martens, who has provided me with this precious opportunity to learn and work in his lab. For the whole time of my practice, he has been very supportive of my project and he was the mastermind who led the main direction of the research. Whenever I hit obstacles or had confusions, he was always willing to listen and explain, and more importantly, inspire me with new ideas and a broader point of view. I have received generous support and encouragement from Dr. Sascha Martens and it will be an important foundation for my future scientific pursuit.

I am especially grateful to Luca Ferrari, who was the most important person that guided and supported me throughout the practice and thesis writing. He designed the framework of my research and taught me every skill that I needed hand by hand with great patience and meticulosity. He generously shared his experience and tips with me and has given me helpful advice whenever I felt stuck. I have followed his lead during the practice and he has been not only a perfect mentor, but also a caring friend to me.

I also want to thank Daniel Bernklau, Justyna Sawa-Makarska, Alberto Danieli, Eleonora Turco, who have helped me with a lot of new methods and lab stuff with warm heart, and discussed with me about my project and provided great ideas. Eleonora Turco and Adriana Savova also shared their p62 and NBR1 proteins with me generously. Julia Romanov and Martina Schuschnig, Stephen Shoebridge were very kind to familiarize me around the lab and support me with everything I needed. Elias Adriaenssens, Verena Baumann, Nicolas Coudevylle, Riccardo Trapannone, David Hollenstein, Bernd Bauer, Sonja Achleitner have made my time in the lab enjoyable.

I felt fully supported in this big family and this work is credited to everyone in the Martens lab.

References

1. Yang, Z. & Klionsky, D. J. Mammalian autophagy: core molecular machinery and signaling regulation. *Curr. Opin. Cell Biol.* **22**, 124–131 (2010).
2. Csizmadia, T. & Juhász, G. Chapter Eleven - Crinophagy mechanisms and its potential role in human health and disease. in *Progress in Molecular Biology and Translational Science* (eds. Martinez, A. B. & Galluzzi, L.) vol. 172 239–255 (Academic Press, 2020).
3. Levine, B. & Klionsky, D. J. Development by Self-Digestion: Molecular Mechanisms and Biological Functions of Autophagy. *Dev. Cell* **6**, 463–477 (2004).
4. Christian, M. Autophagy and antigen presentation. *Cell. Microbiol.* **Volume8**, Pages 891-898 (2006).
5. Shintani, T. & Klionsky, D. J. Autophagy in health and disease: a double-edged sword. *Science* **306**, 990–995 (2004).
6. Zaffagnini, G. & Martens, S. Mechanisms of Selective Autophagy. *J. Mol. Biol.* **428**, 1714–1724 (2016).
7. Mizushima, N. & Komatsu, M. Autophagy: renovation of cells and tissues. *Cell* **147**, 728–741 (2011).
8. Xie, Z. & Klionsky, D. J. Autophagosome formation: core machinery and adaptations. *Nat. Cell Biol.* **9**, 1102–1109 (2007).
9. Kocaturk, N. M. & Gozuacik, D. Crosstalk Between Mammalian Autophagy and the Ubiquitin-Proteasome System |. *Front. Cell Dev. Biol.* (2018).
10. Lee, M. J., Lee, J. H. & Rubinsztein, D. C. Tau degradation: the ubiquitin-proteasome system versus the autophagy-lysosome system. *Prog. Neurobiol.* **105**, 49–59 (2013).
11. Park, C. & Cuervo, A. M. Selective autophagy: talking with the UPS. *Cell Biochem. Biophys.* **67**, 3–13 (2013).
12. Kuma, A. *et al.* The role of autophagy during the early neonatal starvation period. *Nature* **432**, 1032–1036 (2004).
13. Kraft, C., Reggiori, F. & Peter, M. Selective types of autophagy in yeast. *Biochim. Biophys. Acta* **1793**, 1404–1412 (2009).
14. Scrivo, A., Bourdenx, M., Pampliega, O. & Cuervo, A. M. Selective autophagy as a potential therapeutic target for neurodegenerative disorders. *Lancet Neurol.* **17**, 802–815 (2018).
15. Dikic, I., Johansen, T. & Kirkin, V. Selective autophagy in cancer development and therapy. *Cancer Res.* **70**, 3431–3434 (2010).

16. Lamark, T., Kirkin, V., Dikic, I. & Johansen, T. NBR1 and p62 as cargo receptors for selective autophagy of ubiquitinated targets. *Cell Cycle Georget. Tex* **8**, 1986–1990 (2009).
17. Sarraf, S. A. *et al.* Loss of TAX1BP1-Directed Autophagy Results in Protein Aggregate Accumulation in the Brain. *Mol. Cell* **80**, 779-795.e10 (2020).
18. Khaminets, A., Behl, C. & Dikic, I. Ubiquitin-Dependent And Independent Signals In Selective Autophagy. *Trends Cell Biol.* **26**, 6–16 (2016).
19. Chang, C. *et al.* Reconstitution of cargo-induced LC3 lipidation in mammalian selective autophagy. *Sci. Adv.* **7**, eabg4922 (2021).
20. Cabe, M., Rademacher, D. J., Karlsson, A. B., Cherukuri, S. & Bakowska, J. C. PB1 and UBA domains of p62 are essential for aggresome-like induced structure formation. *Biochem. Biophys. Res. Commun.* **503**, 2306–2311 (2018).
21. Matsumoto, G., Wada, K., Okuno, M., Kurosawa, M. & Nukina, N. Serine 403 phosphorylation of p62/SQSTM1 regulates selective autophagic clearance of ubiquitinated proteins. *Mol. Cell* **44**, 279–289 (2011).
22. Long, J. *et al.* Dimerisation of the UBA domain of p62 inhibits ubiquitin binding and regulates NF-kappaB signalling. *J. Mol. Biol.* **396**, 178–194 (2010).
23. Wurzer, B. *et al.* Oligomerization of p62 allows for selection of ubiquitinated cargo and isolation membrane during selective autophagy - PubMed. *eLife* (2015).
24. Danieli, A. & Martens, S. p62-mediated phase separation at the intersection of the ubiquitin-proteasome system and autophagy. *J. Cell Sci.* **131**, jcs214304 (2018).
25. Sun, D., Wu, R., Zheng, J., Li, P. & Yu, L. Polyubiquitin chain-induced p62 phase separation drives autophagic cargo segregation. *Cell Res.* **28**, 405–415 (2018).
26. Savova, A., Romanov, J. & Martens, S. NBR1 directly promotes the formation of p62 – ubiquitin condensates via its PB1 and UBA domains. *bioRxiv* (2020).
27. Dittmar, G. & Winklhofer, K. F. Linear Ubiquitin Chains: Cellular Functions and Strategies for Detection and Quantification. *Front. Chem.* **7**, 915 (2020).
28. Komander, D. & Rape, M. The Ubiquitin Code | Annual Review of Biochemistry. *Annu. Rev. Biochem.* 203–229 (2012).
29. Tan, J. M. M. *et al.* Lysine 63-linked ubiquitination promotes the formation and autophagic clearance of protein inclusions associated with neurodegenerative diseases. *Hum. Mol. Genet.* **17**, 431–439 (2008).
30. Long, J. *et al.* Ubiquitin recognition by the ubiquitin-associated domain of p62 involves a novel conformational switch. *J. Biol. Chem.* **283**, 5427–5440 (2008).
31. Walinda, E. *et al.* Solution structure of the ubiquitin-associated (UBA) domain of human

autophagy receptor NBR1 and its interaction with ubiquitin and polyubiquitin. *J. Biol. Chem.* **289**, 13890–13902 (2014).
32. Ciuffa, R. *et al.* The selective autophagy receptor p62 forms a flexible filamentous helical scaffold. *Cell Rep.* **11**, 748–758 (2015).
33. Sluimer, J. & Distel, B. Regulating the human HECT E3 ligases. *Cell. Mol. Life Sci. CMLS* **75**, 3121–3141 (2018).
34. Hochstrasser, M. Lingering mysteries of ubiquitin-chain assembly. *Cell* **124**, 27–34 (2006).
35. Dye, B. T. & Schulman, B. A. Structural mechanisms underlying posttranslational modification by ubiquitin-like proteins. *Annu. Rev. Biophys. Biomol. Struct.* **36**, 131–150 (2007).
36. Rodrigo-Brenni, M. C., Foster, S. A. & Morgan, D. O. Catalysis of lysine 48-specific ubiquitin chain assembly by residues in E2 and ubiquitin. *Mol. Cell* **39**, 548–559 (2010).
37. Hodge, C. D., Spyracopoulos, L. & Glover, J. N. M. Ubc13: the Lys63 ubiquitin chain building machine. *Oncotarget* **7**, 64471–64504 (2016).
38. Pickart, C. M. Mechanisms underlying ubiquitination. *Annu. Rev. Biochem.* **70**, 503–533 (2001).
39. Mevissen, T. E. T. & Komander, D. Mechanisms of Deubiquitinase Specificity and Regulation. *Annu. Rev. Biochem.* **86**, 159–192 (2017).
40. Weingarten, M. D., Lockwood, A. H., Hwo, S. Y. & Kirschner, M. W. A protein factor essential for microtubule assembly. *Proc. Natl. Acad. Sci. U. S. A.* **72**, 1858–1862 (1975).
41. Jagust, W. Imaging the evolution and pathophysiology of Alzheimer disease. *Nat. Rev. Neurosci.* **19**, 687–700 (2018).
42. Bierer, L. M. *et al.* Neocortical neurofibrillary tangles correlate with dementia severity in Alzheimer's disease. *Arch. Neurol.* **52**, 81–88 (1995).
43. Kovacs, G. G. Tauopathies. *Handb. Clin. Neurol.* **145**, 355–368 (2017).
44. Mazanetz, M. P. & Fischer, P. M. Untangling tau hyperphosphorylation in drug design for neurodegenerative diseases. *Nat. Rev. Drug Discov.* **6**, 464–479 (2007).
45. Brown, M. R., Bondada, V., Keller, J. N., Thorpe, J. & Geddes, J. W. Proteasome or calpain inhibition does not alter cellular tau levels in neuroblastoma cells or primary neurons. *J. Alzheimers Dis. JAD* **7**, 15–24 (2005).
46. Feuillette, S. *et al.* Tau is not normally degraded by the proteasome. *J. Neurosci. Res.* **80**, 400–405 (2005).
47. Hamano, T. *et al.* Autophagic-lysosomal perturbation enhances tau aggregation in

transfectants with induced wild-type tau expression. *Eur. J. Neurosci.* **27**, 1119–1130 (2008).
48. Berger, Z. *et al.* Rapamycin alleviates toxicity of different aggregate-prone proteins. *Hum. Mol. Genet.* **15**, 433–442 (2006).
49. Schaeffer, V. *et al.* Stimulation of autophagy reduces neurodegeneration in a mouse model of human tauopathy. *Brain* **135**, 2169–2177 (2012).
50. Chesser, A. S., Pritchard, S. M. & Johnson, G. V. W. Tau clearance mechanisms and their possible role in the pathogenesis of Alzheimer disease. *Front. Neurol.* **4**, 122 (2013).
51. Kuusisto, E., Salminen, A. & Alafuzoff, I. Early accumulation of p62 in neurofibrillary tangles in Alzheimer's disease: possible role in tangle formation. *Neuropathol. Appl. Neurobiol.* **28**, 228–237 (2002).
52. Kuusisto, E., Salminen, A. & Alafuzoff, I. Ubiquitin-binding protein p62 is present in neuronal and glial inclusions in human tauopathies and synucleinopathies. *Neuroreport* **12**, 2085–2090 (2001).
53. Ramesh Babu, J. *et al.* Genetic inactivation of p62 leads to accumulation of hyperphosphorylated tau and neurodegeneration. *J. Neurochem.* **106**, 107–120 (2008).
54. D'Agostino, C., Nogalska, A., Cacciottolo, M., Engel, W. K. & Askanas, V. Abnormalities of NBR1, a novel autophagy-associated protein, in muscle fibers of sporadic inclusion-body myositis. *Acta Neuropathol. (Berl.)* **122**, 627–636 (2011).
55. Petrucelli, L. *et al.* CHIP and Hsp70 regulate tau ubiquitination, degradation and aggregation. *Hum. Mol. Genet.* **13**, 703–714 (2004).
56. Subramanian, M. *et al.* UBE4B, a microRNA-9 target gene, promotes autophagy-mediated Tau degradation. *Nat. Commun.* **12**, 3291 (2021).
57. Flach, K. *et al.* Axotrophin/MARCH7 acts as an E3 ubiquitin ligase and ubiquitinates tau protein in vitro impairing microtubule binding. *Biochim. Biophys. Acta* **1842**, 1527–1538 (2014).
58. Babu, J. R., Geetha, T. & Wooten, M. W. Sequestosome 1/p62 shuttles polyubiquitinated tau for proteasomal degradation. *J. Neurochem.* **94**, 192–203 (2005).
59. Ferrari, L. & Rüdiger, S. G. D. Recombinant production and purification of the human protein Tau. *Protein Eng. Des. Sel. PEDS* **31**, 447–455 (2018).
60. Ballinger, C. A. *et al.* Identification of CHIP, a novel tetratricopeptide repeat-containing protein that interacts with heat shock proteins and negatively regulates chaperone functions. *Mol. Cell. Biol.* **19**, 4535–4545 (1999).
61. Dou, F. *et al.* Chaperones increase association of tau protein with microtubules. *Proc.*

Natl. Acad. Sci. U. S. A. **100**, 721–726 (2003).
62. Lamark, T. *et al.* Interaction codes within the family of mammalian Phox and Bem1p domain-containing proteins. *J. Biol. Chem.* **278**, 34568–34581 (2003).
63. Bjørkøy, G. *et al.* p62/SQSTM1 forms protein aggregates degraded by autophagy and has a protective effect on huntingtin-induced cell death. *J. Cell Biol.* **171**, 603–614 (2005).
64. Zhang, H. *et al.* A bipartite interaction between Hsp70 and CHIP regulates ubiquitination of chaperoned client proteins. *Struct. Lond. Engl. 1993* **23**, 472–482 (2015).
65. Arakhamia, T. *et al.* Posttranslational Modifications Mediate the Structural Diversity of Tauopathy Strains. *Cell* **180**, 633-644.e12 (2020).
66. Ravalin, M. *et al.* Specificity for latent C termini links the E3 ubiquitin ligase CHIP to caspases. *Nat. Chem. Biol.* **15**, 786–794 (2019).
67. Zaffagnini, G. *et al.* p62 filaments capture and present ubiquitinated cargos for autophagy. *EMBO J.* **37**, e98308 (2018).
68. Turco, E. *et al.* Reconstitution defines the roles of p62, NBR1 and TAX1BP1 in ubiquitin condensate formation and autophagy initiation. *Nat. Commun.* **12**, 5212 (2021).
69. Turco, E. *et al.* FIP200 Claw Domain Binding to p62 Promotes Autophagosome Formation at Ubiquitin Condensates. *Mol. Cell* **74**, 330-346.e11 (2019).
70. Yoon, M. J. *et al.* UXT chaperone prevents proteotoxicity by acting as an autophagy adaptor for p62-dependent aggrephagy. *Nat. Commun.* **12**, 1955 (2021).
71. Harrigan, J. A., Jacq, X., Martin, N. M. & Jackson, S. P. Deubiquitylating enzymes and drug discovery: emerging opportunities. *Nat. Rev. Drug Discov.* **17**, 57–78 (2018).
72. Wang, P. *et al.* Tau interactome mapping based identification of Otub1 as Tau deubiquitinase involved in accumulation of pathological Tau forms in vitro and in vivo. *Acta Neuropathol. (Berl.)* **133**, 731–749 (2017).
73. Wang, J.-Z., Xia, Y.-Y., Grundke-Iqbal, I. & Iqbal, K. Abnormal hyperphosphorylation of tau: sites, regulation, and molecular mechanism of neurofibrillary degeneration. *J. Alzheimers Dis. JAD* **33 Suppl 1**, S123-139 (2013).
74. Liu, M. *et al.* Hyperphosphorylation Renders Tau Prone to Aggregate and to Cause Cell Death. *Mol. Neurobiol.* **57**, 4704–4719 (2020).
75. Liu, F., Liang, Z. & Gong, C. X. Hyperphosphorylation of tau and protein phosphatases in Alzheimer disease. *Panminerva Med.* **48**, 97–108 (2006).
76. Wesseling, H. *et al.* Tau PTM Profiles Identify Patient Heterogeneity and Stages of Alzheimer's Disease. *Cell* **183**, 1699-1713.e13 (2020).